RAPID KINETIC STUDIES OF PHYA FROM *SELENOMONAS RUMINANTIUM*, AND A SIMPLIFIED MEANS OF PRODUCTION OF A PHOSPHATE BIOSENSOR

Dustin D. Smith
Bachelor of Science, University of Lethbridge, 2013

A Thesis
Submitted to the School of Graduate Studies
of the University of Lethbridge
in Partial Fulfillment of the
Requirements for the Degree

MASTER OF SCIENCE
(Biochemistry)

Department of Chemistry and Biochemistry/ Department of Biological Sciences
University of Lethbridge
LETHBRIDGE, ALBERTA, CANADA

RAPID KINETIC STUDIES OF PHYA FROM SELENOMONAS RUMINANTIUM, AND A SIMPLIFIED MEANS OF PRODUCTION OF A PHOSPHATE BIOSENSOR

DUSTIN D. SMITH

Date of Defence: Dec. 16, 2016

Dr. Hans-Joachim Wieden Co-Supervisor	Professor	Ph.D.
Dr. L. Brent Selinger Co-Supervisor	Professor	Ph.D.
Dr. Steven Mosimann Thesis Examination Committee Member	Associate Professor	Ph.D.
Dr. Wade Abbott Thesis Examination Committee Member	Adjunct Professor	Ph.D.
Dr. Rene Boere Chair, Thesis Examination Committee	Professor	Ph.D.

Abstract

Myo-inositol polyphosphates (IPs) are ubiquitous in nature and involved in various cellular events. Dephosphorylation of IPs by protein tyrosine phosphatase-like polyphosphatases (PTPLPs) occurs via a complex pathway, and the *in vivo* function of many of these enzymes remains unknown. In order to further our understanding of PTPLP catalyzed dephosphorylation of IPs; I present rapid kinetics studies of the representative PTPLP PhyA from *Selenomonas ruminantium* (PhyAsr). These studies revealed kinetic parameters of PhyAsr dimerization, and *myo*-inositol hexa*kis*phosphate (IP_6) binding to the homodimer. In addition to studying PhyAsr, I have developed a simplified methodology to produce a biosensor capable of detecting phosphate release in real-time. The phosphate biosensor is fluorescently labeled and utilizes *Escherichia coli* Phosphate-binding protein (PhoS). The results show that my proposed methodology yields a functional biosensor and is feasible for large-scale production. I envision this methodology to be versatile and useful for a large number of research applications where detection of free phosphate is required.

Acknowledgements

I would like to thank Brent Selinger and HJ Wieden for giving me this learning opportunity and supervising me during my time as a Master's student. Thank you to my committee members, Wade Abbott and Steven Mosimann, for your useful feedback and ideas relating to my project. As well I would like to thank Ute Kothe, and the Alberta RNA Research and Training Institute for the use of their lab equipment and resources.

I would like to thank the past and present members of the Kothe, Mosimann, Selinger, and Wieden labs for any assistance they have provided over the past few years.

I would also like to thank my friends and family for their support, and the good times we have had together. I would like to thank my wonderful girlfriend for all of the memories we have shared, and for always making me, "two dots and a U" :)

Table of Contents

List of Tables

Chapter 1

Chapter 3

Chapter 4

List of Figures

Chapter 1

Chapter 2

Chapter 3

Chapter 4

List of Abbreviations

5-IAF	5-iodoacetamidofluorescein
50S	50 svedberg prokaryotic ribosome
70S	70 svedberg prokaryotic ribosome
ABC	ATP-binding cassette
ADP	Adenosine diphosphate
ATP	Adenosine triposphate
A.U.	Arbitrary Units
BLASTp	Basic Local Alignment Search Tool (protein sequence input)
BME	β-mercaptoethanol
BPPs	β-Propeller phytases
DMF	dimethylformamide
EDTA	ethylenediaminetetraacetic acid
HAP	Histidine acid phosphatase
IMAC	Immobilized metal affinity chromatography
IP	*myo*-inositol polyphosphate
IP_3	*myo*-inositol-1,4,5-triphosphate
IP_4	*myo*-inositol-1,2,5,6-tetraphosphate
IP_5	*myo*-inositol-1,2,4,5,6-pentakisphosphate
IP_6	*myo*-inositol hexakisphosphate
IPase	*myo*-inositol polyphosphate-degrading enzymes
IPTG	isopropyl β-D-1-thiogalactopyranoside
K_D	Equilibrium dissociation constant
K_M	Michaelis constant
MAPK	Mitogen-activated protein kinase
MDCC	N-[2-(1-maleimidyl)ethyl]-7-(diethylamino)coumarin-3-carboxamide
P_i	inorganic phosphate
PAP	Purple acid phosphatases
PDE	Phytate-Degrading Enzyme
PhoS	Phosphate binding protein from *Escherichia coli*
PhyAbb	PhyA from *Bdellovibrio bacteriovorus*
PhyAcp	PhyA from *Clostridium perfringens*
PhyAdm	PhyA from *Desulfovibrio magneticus*
PhyAlpp	PhyA from *Legionella pneumophila* str. *Paris*
PhyAme	PhyA from *Megasphaera elsdenii*
PhyAmm	PhyA from *Mitsuokella multacidia*
PhyAms	PhyA from *Myxococcus stipitatus*
PhyAsl	PhyA from *Selenomonas lacticifex*
PhyAsr	PhyA from *Selenomonas runinantium*
PhyAsrl	PhyA from *S. ruminantium* subspecies *lactilytica*
PhyBmm	PhyB from *Mitsuokella multacidia*
PhyBsl	PhyB from *Selenomonas lacticifex*
PIP	phosphatidylinositol phosphate
PMSF	phenylmethylsulfonylfluoride
pre-PhoS	PhoS with its N-terminal signal sequence
PST	Phosphate specific transport

PTP	Protein tyrosine phosphatase
PTPLP	Protein tyrosine phosphatase-like polyphosphatases
rho	tetramethylrhodamine
SDS PAGE	sodium dodecyl sulfate polyacrylamide gel electrophoresis
Tris	Tris(hydroxymethyl)aminomethane

Chapter 1: Literature Review: *myo*-inositol polyphosphate-degrading enzymes

1.1 *myo*-inositol polyphosphates

Myo-inositol polyphosphates (IPs) are ubiquitous in nature and involved in a number of important cellular signalling events (Best et al., 2010). There are a total of 63 possible permutations of the IP molecule, excluding IPs with pyrophosphate groups; and altering the phosphorylation state of an IP can trigger various events *in vivo* due to different phosphorylation patterns of IPs having a variety of signalling roles. However, it is not clear if IPs play a role in cell signalling in bacteria, as IPs have yet to be identified in this group of organisms. Of the IPs, *myo*-inositol hexakisphosphate (IP_6, or phytate) is the most abundant *in vivo* and can have a number of roles in different cell types (Best et al., 2010). For example IP_6 can be involved in RNA processing, mRNA export, DNA repair, apoptosis, plant development, and bacterial pathogenicity (York et al., 1999, Hanakahi et al., 2000, Chatterjee et al., 2003, Macbeth et al., 2005, Tan et al., 2007, Majerus et al., 2008). Additionally, IP_6 is utilized as a phosphate storage molecule in some organisms (Raboy and Dickinson 1987).

IPs with lower phosphorylation states can also serve important roles. *Myo*-inositol-1,3,4,5,6-pentakisphosphate is involved in cell proliferation, chromatin remodelling, viral assembly, and calcium channel regulation (Caffrey et al., 2001, Campbell et al., 2001, Quignard et al., 2003, Steger et al., 2003, Orchiston et al., 2004, Piccolo et al., 2004, Maffucci et al., 2005). As well, *myo*-inositol-1,4,5-triphosphate (IP_3) has been shown to have a role as a second messenger in calcium release (Streb et al., 1983, Best et al., 2010).

IPs can also be components of other important molecules involved in signal transduction pathways. For example, phosphatidylinositol phosphates (PIPs) consist of a glycerophospholipid attached to a phosphorylated *myo*-inositol head group (Best et al., 2010). The position(s) that are phosphorylated on the *myo*-inositol head group can vary, and these structures are important in cell signalling, and membrane trafficking (Di Paolo and De Camilli 2006, Wymann and Schneiter 2008, Posor et al., 2013).

1.1.1 *myo*-inositol polyphosphate structure

The structure of an IP is an achiral (meso) cyclohexane that can be phosphorylated at different positions (Best et al., 2010). Research utilizing nuclear magnetic resonance spectroscopy of 0.1 M solutions of the $Na_{12}IP_6$ salt have shown that for IP_6 the most energetically favorable conformation adopts a 5-equatorial/1-axial conformation at pH values less than 9.2 (Isbrandt and Oertel 1980). At pH values larger than 9.6, IP_6 undergoes a pH dependent inversion and adopts a 5-axial/1-equatorial conformation (Isbrandt and Oertel 1980). However, the conformational properties of IP_6 can be strongly influenced by counter ions (Bauman et al., 1999), so that the aforementioned pH values causing conformational inversion of IP_6 should not be treated as absolute. A numbering convention commonly adopted labels the 1-position on the inositol ring as the point where the inositol ring is attached to a lipid backbone in inositol-based lipid structures. Numbering then continues counter-clockwise in the inositol ring, starting with the 2-position at the only axial group present in the < 9.2 pH structure of IP_6 (Best et al., 2010). This is the "D" numbering system for IPs (Fig. 1.1), and because the majority of biologically active IPs are the "D" enantiomers most researchers utilize the "D" numbering methodology (Murthy 2006).

When IP_6 is at physiological pH it has a charge between -6 and -9 (Isbrandt and Oertel 1980). This negative charge allows IP_6 to associate with a variety of positively charged entities, including cations or electropositive regions on proteins (Macbeth et al., 2005, Tan et al., 2007, Lupardus et al., 2008). Twelve sites on IP_6 can be protonated, six of these protons have pK_a values of approximately 1.8; three protons have pK_a values between 6.0 and 7.6, and the last three protons have pK_a values between 9.2 and 9.6 (Isbrandt and Oertel 1980). However, these pK_a values may vary depending on the presence and concentration of cations.

1.2 *myo*-inositol polyphosphate-degrading enzymes

Myo-inositol polyphosphate-degrading enzymes (IPases) are enzymes which catalyze the dephosphorylation of IPs via phosphoester bond hydrolysis, generating lower order IPs (Chen et al., 2015). IPases have been identified in prokaryotes and eukaryotes, and have a number of proposed roles as the hydrolysis of phosphate esters is involved in many cellular processes (Chen et al., 2015). For example, some plants are hypersusceptible to viral infections when their IP_6 levels are low, and an IPase from the plant pathogen *Xanthomonas oryzae* is secreted and acts as a virulence factor by degrading host IP_6 (Chatterjee et al., 2003, Murphy et al., 2008). Some IPases have been shown to be exported from the cell and associated with the outer membrane, potentially suggesting a role in phosphate scavenging (D'Silva et al., 2000). Additionally, low phosphate levels in culture medium are required for the transcription of some IPase genes, further suggesting a role in phosphate scavenging (Van Hartingsveldt et al., 1993).

IPases that can dephosphorylate phytate are generally referred to as phytases. Phytases can have narrow or broad substrate specificities, and enzymes with broad substrate specificity may not utilize IPs as their preferred substrate (Rossburger et al., 2012). Additionally, the order of the dephosphorylation pathway of a substrate with multiple phosphate groups can vary (Table 1.1). Knowledge of the substrate specificity of phytases is key to understanding its *in vivo* function, as well as its biochemical properties. Moreover, the divergence of substrate specificity within the phytases, or within a class of phytases, is an interesting topic from an evolutionary and enzyme engineering perspective.

1.2.1 Classification of Phytases

All known phytases currently fall into one of four groups: histidine acid phosphatases, β-propeller phytases, purple-acid phosphatases, and protein tyrosine phosphatase-like phytases (Chen et al., 2015). Although these enzymes all share the ability to degrade IP_6, their mechanisms of action, structural features, and substrate specificities differ (Chen et al., 2015).

1.2.1.1 Histidine Acid Phosphatases

Histidine Acid Phosphatases (HAPs) represent the majority of phytases characterized to date (Chen et al., 2015). This group of enzymes has significant importance to agriculture, as the HAPs are often used as feed supplements in monogastric livestock diets to increase phosphate availability by breaking down plant-derived IPs (Mullaney et al., 1999). A two-step mechanism has been proposed to describe the liberation of phosphate from an IP by a HAP. The foundation of this two-step mechanism

hypothesis has been formed on crystallographic studies of transition-state complexes, and site-directed mutagenesis (Ostanin et al., 1992, Ostanin and Van Etten 1993, Lim et al., 2000, Liu et al., 2004). The proposed two-step mechanism involves first positioning of the scissile phosphate by its interaction with a conserved Arg in the active site. A conserved His of the "RHGXRXP" active site signature sequence acts as a nucleophile and forms a phospho-histidine intermediate. Next, a conserved Asp of the "HD" motif protonates the leaving group, and a water molecule hydrolyzes the covalent intermediate releasing the catalytic His for subsequent reactions (Ostanin et al., 1992, Ostanin and Van Etten 1993, Chen et al., 2015).

Both prokaryotic and eukaryotic HAPs have been identified, and aside from the aforementioned active site sequence motifs they share little sequence similarity. To date, a total of 25 HAP crystal structures have been reported from 9 organisms. HAP structural data shows that these proteins contain a α/β domain, and a smaller α domain, where substrate binding occurs at an interface between these two domains. Substrate specificity also varies between the HAPs, as diversity exists in the preferred ligands utilized by this group of enzymes (Chen et al., 2015). Divergence in quaternary structure has also been observed between the HAPs, as two of the studied proteins crystalize as a tetramer (Kostrewa et al., 1999, Ragon et al., 2009).

1.2.1.2 β-Propeller Phytase

β-Propeller phytases (BPPs) were first identified in *Bacillus* species, and fold into a six-bladed β-propeller structure (Ha et al., 2000). Also of structural importance to the BPPs are Ca^{2+} ions, which are required both for protein thermostability and activity

(Kerovuo et al., 2000). The binding of an IP to the BPP binding pocket is distinct from other phytases in that it requires Ca^{2+} ions to provide favourable electrostatic interactions (Oh et al., 2001). This information combined with the absence of active site sequence conservation with HAPs suggests a unique mechanism of IP dephosphorylation by BPPs. Recent research has identified novel BPP candidate enzymes via survey of the intestinal contents of grass carp, with many distinct BPP genes originating from uncultured microorganisms (Huang et al., 2009). BPPs have been found broadly distributed in soil bacteria, plant bacteria, and aquatic environments; and may play a role in phytate-phosphate cycling (Lim et al., 2007).

1.2.1.3 Purple-Acid Phosphatases

Two phytate-degrading enzymes from *Aspergillus niger,* and *Glycine max* with homology to purple-acid phosphatases (PAPs) have also been studied (Ullah and Cummins 1988, Hegeman and Grabau 2001). Of these enzymes, the protein from *G. max* shows significantly more activity against phytate (Mullaney and Ullah 2003). PAPs are a class of metallophosphoesterases, which utilize Fe (III) metal ions in combination with Fe (II), Mn (II), or Zn (II) to form a binuclear metal center. The dephosphorylation mechanism used by PAPs first involves interaction between the substrate and the divalent cation of the binuclear center. Next, an Fe (III)-coordinated hydroxide performs a nucleophilic attack on the scissile phosphate (Klabunde et al., 1996).

1.2.1.4 Protein Tyrosine Phosphatase-like Phytases

The most recently discovered subgroup of IPases, protein tyrosine phosphatase-like phytases (PTPLPs) are predominantly microbial enzymes which contain a protein

tyrosine phosphatase (PTP)-like active site signature sequence ($C(X)_5R(S/T)$). PTPLPs are believed to utilize a similar dephosphorylation mechanism as PTPs due to the similarity of conserved active site features (Gruninger 2009). The mechanism of PTP catalyzed dephosphorylation has been proposed to proceed via a two-step mechanism (Guan and Dixon 1991, Zhang 2003). In the first step, a nucleophillic P-loop cysteine attacks the scissile phosphate of the substrate, while an aspartic acid protonates the leaving group. The transition state complex is stabilized by the aforementioned aspartic acid, an active site arginine, and main chain amines of the P-loop (Hengge et al., 1995, Zhang 2003). This results in the formation of a covalent phospho-cysteine intermediate (Guan and Dixon 1991, Pannifer et al., 1998). The second step in the reaction mechanism involves positioning a water molecule for nucleophillic attack by the same aspartic acid from the first step, followed by hydrolysis of the covalent intermediate (Wu and Zhang 1996, Zhang 2003).

Of the PTPLPs characterized, one of the two domains adopts a PTP-like fold while the other is a unique phytase domain (Chu et al., 2004, Gruninger et al., 2012, Gruninger et al., 2014). The significance of the evolutionary relationship between PTPs and PTPLPs is currently unknown; however, the best studied eukaryotic PTPs serve as regulators of cellular function (Shi et al., 1998). Currently, many PTPLPs have been hypothesized to be involved in phosphate scavenging or cell signalling; however, specific roles remain unknown for all but HopAO1 from the phytopathogen *Pseudomonas syringae*. HopAO1 contains a C-terminal PTPLP domain, and an N-terminal avirulence region used by type-III secretion systems to transport HopAO1 into plant cells (Espinosa et al., 2003). HopAO1 has been proposed to be a virulence factor for *P. syringae* that

suppresses apoptosis in plant cells, likely by interference with the Mitogen-activated protein kinase (MAPK) pathway (Bretz et al., 2003, Espinosa et al., 2003, Macho et al., 2014). As well, a PTPLP from *Legionella pneumophila* str. *Paris* has a similar proposed function through a type-IV secretion system (Weber et al., 2014).

1.3 Recent Protein Tyrosine Phosphatase-like Phytase Research

PTPLPs from various organisms have been cloned into *E. coli,* and their protein products characterized using several *in vitro* enzyme assays (Gruninger et al., 2003, Puhl et al., 2007, Puhl et al., 2008a, Puhl et al., 2008b, Puhl et al., 2009, Thibault 2010, Rossburger et al., 2012, Gruninger et al., 2014, Van Herk et al., 2015). The characterization of PTPLPs from anaerobic Gram-positive bacteria has included: PhyAsr from *Selenomonas ruminantium*, PhyAmm and PhyBmm from *Mitsuokella multacida*, PhyAsl and PhyBsl from *Selenomonas lacticifex*, PhyAsrl from *S. ruminantium* subspecies *lactilytica*, PhyAme from *Megasphaera elsdenii*, and PhyAcp from *Clostridium perfringens*. PTPLPs from Gram-negative bacteria have also been characterized, including: HopAO1 from *Pseudomonas syringae* pv. *tomato*, PhyAbb from *Bdellovibrio bacteriovorus*, PhyAlpp from *Legionella pneumophila* str. *Paris*, PhyAdm from *Desulfovibrio magneticus*, and PhyAms from *Myxococcus stipitatus*. Biochemical properties of these PTPLPs have been summarized (Table 1.1). To date, over 300 homologs to PhyAsr from various bacterial organisms have been identified. In order to show the diversity and evolutionary trajectory of the PTPLP class of enzymes, a phylogenetic tree of the PTPLP genes from these organisms has been constructed (Fig. 1.2). By characterizing the substrate binding properties of various enzymes on the tree, one can describe the divergence of substrate specificity within this class of enzymes. With

this type of data set, researchers are better equipped to develop methods to produce specific IPs of interest. For example, either by engineering an enzyme to have novel functionality, or by predicting which uncharacterized PTPLPs in the tree will have a desired activity.

The PTPLPs characterized tend to have acidic pH optima in the range of 4 - 6, and temperature optima of 40 – 60 °C. An exception to this is HopAO1, which has a neutral pH optimum and operates best at mesophilic temperatures. In studies screening 20 phosphorylated substrates, PTPLPs generally were most active against IP_6. However, two PTPLPs – PhyAcp and PhyBmm – showed broad substrate specificity and displayed more activity against substrates other than IP_6 (Rossburger et al., 2012). Other than PhyAcp and PhyBmm, PTPLPs showed little or no activity against conventional PTP substrates (e.g. O-phospho-tyrosine), and it has been suggested that various structural features confer specificity for IPs (Chu et al., 2004, Puhl et al., 2007, Puhl et al., 2008a).

A parameter that has often been examined when studying PTPLPs is their dephosphorylation pathway of IP_6. Most PTPLPs have a single, specific dephosphorylation pathway of IP_6 that is followed more than 80% of the time. An exception to this is PhyAme, which has two prominent dephosphorylation pathways. These primary dephosphorylation pathways can differ for each PTPLP, and alternate minor pathways exist for IP dephosphorylation. For inositol-based substrates there appears to be a preference for the more highly phosphorylated substrate, as PTPLPs generally display the most activity towards IP_6 (Table 1.1). Preference for the more

negatively charged phosphorylated substrates may be for electrostatic reasons, as many PTPLP binding pockets contain electropositive regions that interact with substrate (Gruninger et al., 2009, Gruninger et al., 2012, Gruninger et al., 2014). Of the PTPLPs with known IP_6 dephosphorylation pathways, all are able to remove 5 phosphate groups leaving a singly substituted IP with a phosphate at the 2-position; except for HopAO1, which removes fewer than 5 phosphates from IP_6. There are two PTPLPs that have shown preference for lower order IPs over IP_6. These enzymes are PhyBsl, and the D1 domain of PhyAmm (Puhl et al., 2008a, Gruninger et al., 2009). The basis of *myo*-inositol-1,2,5,6-tetraphosphate (IP_4) substrate preference by PhyBsl is unknown (Puhl et al., 2008a). However, in PhyAmm, activity of the D1 domain is hindered by the presence of a phosphate group at the 2-position on an IP; and docking studies have suggested that this is for steric reasons (Gruninger et al., 2009). Naming of the phytase enzymes may require further consideration, as some enzymes classified as phytases may have very little activity against phytate.

Ongoing PTPLP research projects aim to understand enzyme characteristics with the long-term goal of producing a variety of IP substrates (Van Herk 2014, Chen et al., 2015). Production of these various IP substrates from IP_6 could be achieved by discovering novel activity in uncharacterized PTPLPs, or by modifying the activity of a previously characterized PTPLP to alter its IP degradation pathway. Expanding the scope of IPs that can be produced by PTPLPs will be useful for industrial purposes as an alternative to current production methods, as current chemically synthesized IPs can be very expensive. For example, 1 mg of *myo*-inositol 1,3,4,5 – tetraphosphate from Cayman Chemical currently costs $351 (Cayman Chemical P/N: 60980). Novel PTPLPs have been

identified via survey of ruminant fluid from cattle or by searching genetic and protein databases for relatedness in primary sequence to known PTPLPs (Yanke et al., 1998, Thibault 2010). Although both approaches have resulted in the identification of novel PTPLPs in the past, primary sequence analysis is much less laborious particularly with the rapid accumulation of whole genome sequences in GenBank.

1.3.1 PhyA from *Selenomonas ruminantium*

Much of the PTPLP data available has been derived from studies of the representative PTPLP PhyAsr. PhyAsr was first discovered in a survey of anaerobic ruminal bacteria (Yanke et al., 1998, Yanke et al., 1999). Previous research has shown that PhyAsr is exported from *S. ruminantium* and associates to the outer cell membrane, suggesting a role in phosphate scavenging (D'Silva et al., 2000). Alternatively, PhyAsr may be involved in some unknown processes where production of specific IPs is required.

The dephosphorylation pathway of PhyAsr has been previously studied by incubating enzyme with substrate, followed by a time-course of IPs produced (Puhl et al., 2007). Results from this study showed that PhyAsr dephosphorylation of IP_6 is very ordered and follows a single, primary pathway greater than 80% of the time (Fig. 1.3). After each phosphate cleavage event, the IP product is released from the binding site and can later re-bind and serve as a substrate for subsequent rounds of hydrolysis. Current hypotheses have proposed that PhyAsr has multiple, overlapping binding sites for IPs; and the primary dephosphorylation pathway is a reflection of the IP permutations best-suited for these sites (Gruninger et al., 2012). Generally speaking, PhyAsr is most active against IPs with more phosphate groups. It has been proposed that this activity is due to

electrostatic interactions as the PhyAsr binding pocket is very electropositive and the more highly substituted IPs harbour a larger negative charge.

Early crystallographic structural studies of PhyAsr in complex with the inhibitor *myo*-inositol hexasulphate showed the active site was located near a conserved Cys-containing P-loop (Chu et al., 2004). Additional crystallographic studies have shown catalytically inactive PhyAsr in complex with various IP substrates revealing the underlying features of its protein architecture (Puhl et al., 2007, Gruninger et al., 2008, Gruninger et al., 2012). This protein folds into a two-domain structure, comprised of a PTP-domain, and a smaller phytase domain. The larger domain is comprised of a 4-stranded β-sheet core surrounded by several α-helices, and the smaller domain consists of a 5-stranded β-sheet and an α-helix. Binding of IPs occurs at an interface between the two domains in close proximity to the P-loop (Fig. 1.4). This protein is also known to crystalize as a homodimer (Gruninger 2009); however, the biological significance of this quaternary structure formation has not been investigated so far.

In addition to structural data, preliminary kinetics and binding studies have been performed using PhyAsr (Gruninger et al., 2012). This enzyme has a K_M value that is several orders of magnitude larger than its K_D, suggesting that it does not follow a Michaelis-Menten mechanism. In order to study binding and rapid kinetics, PhyAsr mutants have been designed that can be labeled with a fluorescent thiol-reactive probe at a position near the IP binding site (either H188C or K301C, Fig. 1.4), and that produce a detectable change in fluorescence upon substrate binding. In previous publications, a catalytically inactive H188C/C252S variant of PhyAsr has been used to obtain

preliminary substrate binding, and rapid kinetics data (Gruninger et al., 2012). This data has suggested that: 1) The affinity of IP_6 for PhyAsr H188C/C252S is less than 1 micromolar; and 2) binding of IP_6 to PhyAsr H188C/C252S follows a mechanism with at least two steps. However, there is no published kinetic data about the formation of the PhyAsr homodimer. Additionally, only limited information is available regarding the kinetics of substrate binding, catalysis, and product release of IPs from PhyAsr. Obtaining kinetic data with respect to the mechanism of PhyAsr will provide insight into the complex nature of the dephosphorylation pathway of this enzyme. Additionally, kinetic studies could be expanded beyond the model system of PhyAsr and utilized with other PTPLPs to examine a broader research objective of examining divergence of substrate specificity.

1.4 Objectives: *myo*-inositol polyphosphate degrading enzymes

As part of my thesis objectives, I have described the kinetic parameters involved in the formation of PhyAsr quaternary structure. This was of interest to me because the formation of PhyAsr dimers may play a role in its *in vivo* functions. As well, this research will allow for improved design of future PhyAsr experiments. For example, various experiments have been published for PhyAsr where the concentration of protein varies greatly between studies; meaning the partitioning of PhyAsr between the different quaternary structure may vary between studies. Additionally in my thesis, I have described the kinetic parameters of IP_6 binding to dimerized PhyAsr. This is a first step in describing the kinetic mechanism of the model PTPLP PhyAsr; however the concentrations of PhyAsr used in these experiments were higher than what has been used in previous research. As well, I have done research on the effect of phosphate on the

binding of IP_6 to PhyAsr. Previous studies have shown that phosphate is an inhibitor of PhyAsr catalyzed dephosphorylation of IP_6; however the mechanistic basis for this inhibition is unknown (Gruninger et al., 2012). In general, these studies will contribute to the overall understanding of the underlying kinetic features of PhyAsr, as well as provide a model system for future PTPLP kinetic studies.

1.5 Chapter 1. Figures and Tables

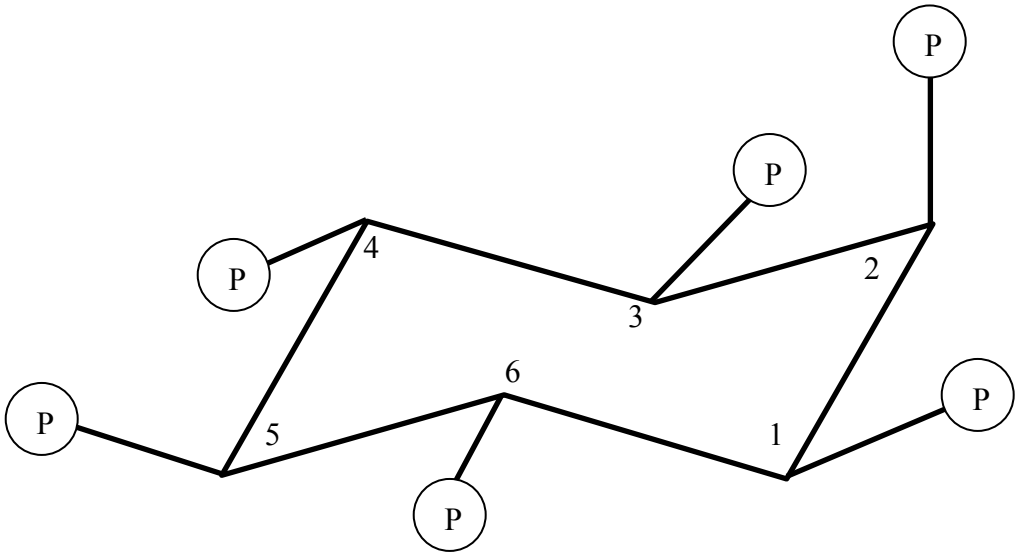

Figure 1.1. Molecular diagram of *myo*-inositol 1,2,3,4,5,6-hexakisphosphate in the chair conformation labeled using the "D" numbering system. Phosphate groups are shown as P, and carbons are numbered inside of the ring. The lone axial phosphate in the < 9.2 pH structure is attached to the carbon numbered as 2, and an internal plane of symmetry runs through the carbons numbered 2 and 5 in this achiral (meso) cyclohexane.

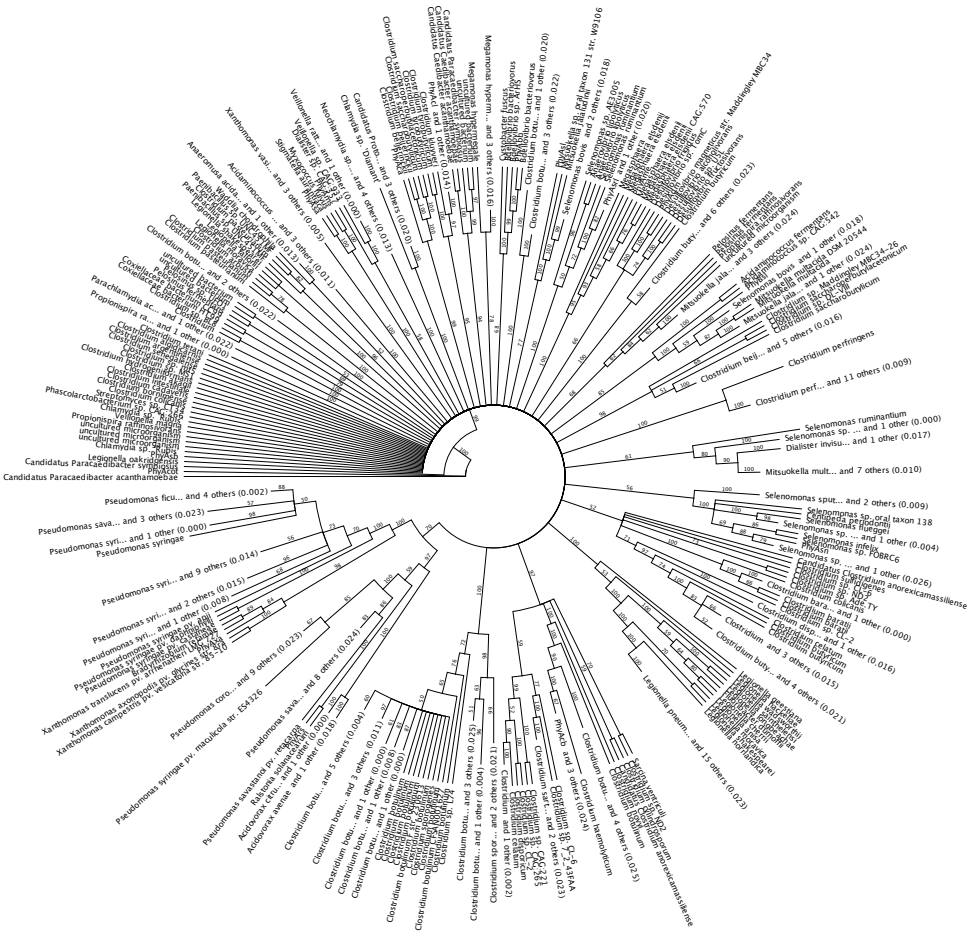

Figure 1.2. Phylogenetic tree of PTPLPs. Phylogenetic tree was constructed using the protein sequence for PhyAsr (Genbank: AAQ13669) as input for Geneious R8. PhyAsr protein sequence was used to perform a BLASTp (Basic Local Alignment Search Tool) with default parameters (database, nr; results, hit table; matrix, BLOSUM62; gap cost, open, 11; gap cost extend 1) (Johnson et al., 2008). Sequences were aligned using a ClustalW alignment with default parameters (cost matrix, BLOSUM; gap open cost, 10; gap extend cost, 0.1), and a tree was built using a neighbour joining distance matrix (Thompson et al., 1994).

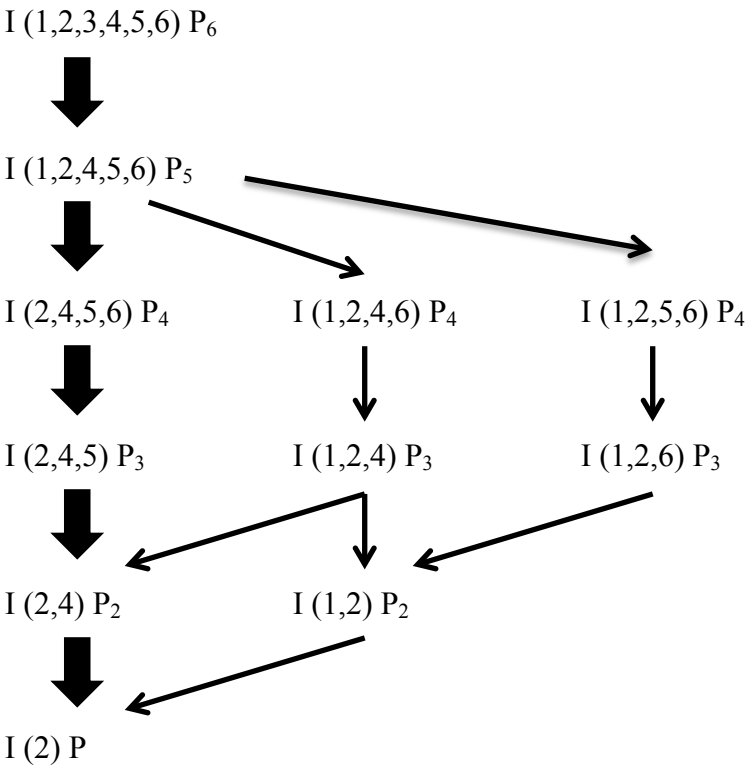

Figure 1.3. The dephosphorylation pathway of IP_6 by PhyAsr. Numbers in brackets denote the position(s) of phosphate groups remaining on the IP. Thicker arrows denote the primary dephosphorylation pathway which has >80% prevalence, and thinner arrows denote minor pathways (Puhl et al., 2007).

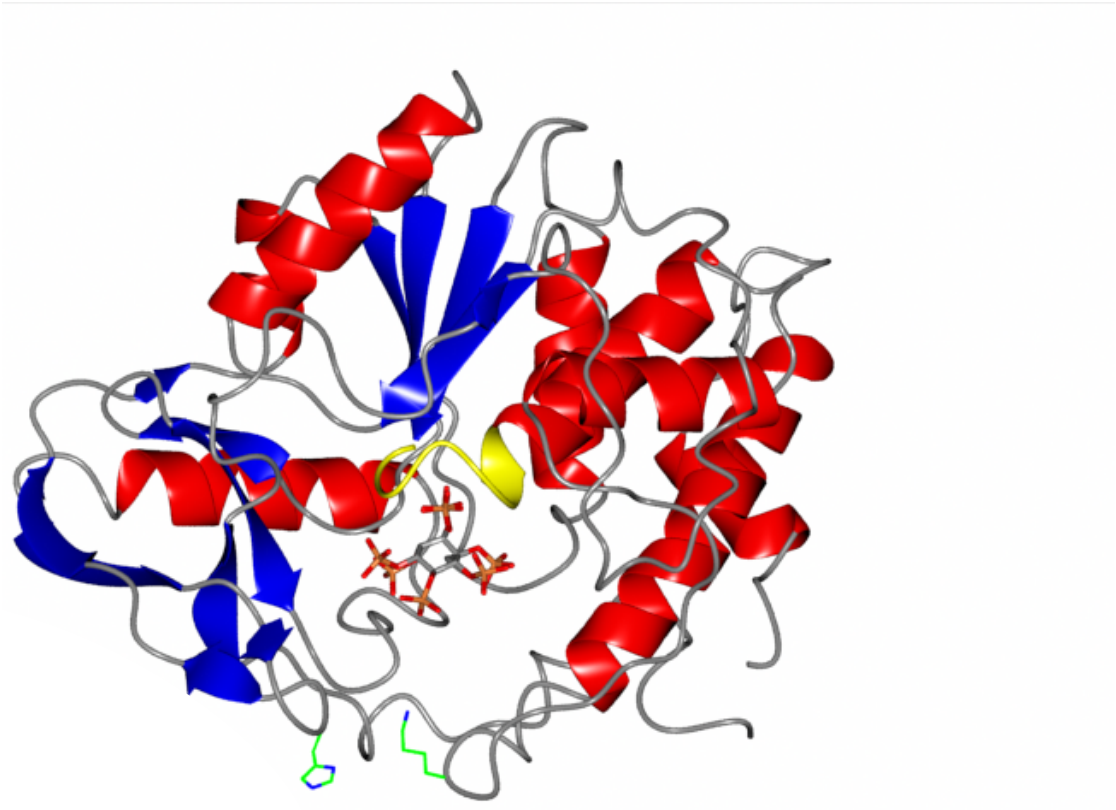

Figure 1.4. Cartoon representation of PhyAsr structure. Colouring is as follows: α-helices – red, β-sheets – blue, P-loop – yellow, positions mutated for fluorescent labeling (H188 or K301) – green. In this structure, a catalytically inactive variant of PhyAsr (C252S) was used, and the IP_6 substrate is visible just below the P-loop. PDB ID: 3MMJ

Table 1.1. Biochemical properties of characterized PTPLPs

Protein	Size (kDa)	Temp. Optimum (°C)	pH Optimum	Substrate Specificity	K_M (μM)	k_{cat} (s^{-1})	IP_6 Degradation Pathway[1]
PhyAsr[2]	40	55	5.0	IP_6	454	608	3,1,6,5,4
PhyAmm[3]	72	60	5.0	IP_6	658	1109	3,1,5,6,4
PhyAsl[4]	35	40	4.5	IP_6	283	245	3,4,5,6,1
PhyBsl[4]	29	40	4.5	IP_4	354	18	3,4,5,6,1
PhyAsrl[5]	32	55	4.5	IP_6/ATP	7/229	8/14	5,4,6,3,1
PhyAme[6]	38	60	5.0	IP_6	64	122	3,4,5,6,1 or 4,5,6,1,3
HopAO1[7]	54	25	7.0	IP_6	63	2	5,6,2
PhyAbb[7,8]	34	50	4.0	IP_6	574	124	NR
PhyAms[9]	33	50	7.5	IP_6	74	<<1	NR
PhyAcp[10]	32	50	3.0	Broad	NR	NR	NR
PhyAdm[10]	35	55	6.0	IP_6	NR	NR	NR
PhyAlpp[10]	34	55	5.5	IP_6	NR	NR	NR
PhyBmm[10]	33	40	5.5	Broad	NR	NR	NR

[1] Numbers indicate the order the phosphate groups are removed
[2] (Puhl et al., 2007)
[3] (Gruninger et al., 2003)
Note: PhyAmm contains multiple active sites with different activities, and the values displayed here reflect the enzyme activity as a whole
[4] (Puhl et al., 2008a)
[5] (Puhl et al., 2008b)
[6] (Puhl et al., 2009)
[7] (Thibault 2010)
[8] (Gruninger et al., 2014)
[9] (Van Herk et al., 2015)
[10] (Rossburger et al., 2012)
N.R. – Not Reported
Note: all protein characterization was performed on constructs lacking signal sequences, and the molecular weights listed reflect constructs lacking signal peptides

Chapter 2: Literature Review: Phosphate detection methods

The detection of free phosphate is a critical element in many biochemical studies. For example, many *in vitro* enzyme activity assays require reliable and quantitative measurement and detection of phosphate concentration. Such assays include the measurement of phosphatase activity, for example the measurement of ATPase, or GTPase activity. Current methods to quantify phosphate for *in vitro* enzyme activity assays include colorimetric chemical assays, radioactive assays, and fluorescence-based detection using labeled phosphate binding protein (Brune et al., 1994, Feng et al., 2011, Craig et al., 2014).

The malachite green-based detection of phosphate is a commonly used colorimetric method (Feng et al., 2011). A typical protocol using this system in an enzyme activity assay would first incubate the enzyme of interest with the respective substrate, followed by quenching of the reaction with strong acid at a specific time point to acquire a time series. Subsequently, the samples will be mixed with malachite green solution, and ammonium molybdate solution, which forms a chromogenic complex in the presence of free phosphate (Feng et al., 2011). The incubation steps are generally 15 – 30 minutes in duration and have involved adding malachite green solution followed by ammonium molybdate solution; alternatively both solutions can be added to the sample at the same time (Feng et al., 2011). The chromogenic complex formed can then be detected by absorbance spectroscopy at 650 nm, and the phosphate concentration in the respective sample can be extrapolated from a previously determined standard curve of A_{650} versus phosphate concentration. This method is versatile, and has been successful for the detection of phosphate concentrations down to the nanomolar range (Hess and Derr

1975). With respect to its use in the kinetic analysis of enzymes, the malachite-based approach can be used for a wide range of experimental designs, such as detection of phosphate formation in ATPases, GTPases, or other phosphatase activity assays. Activity assays can also be expanded to determine other biochemical parameters of enzymes of interest. For example, pH, temperature, or substrate concentration could be varied to determine pH optima, temperature optima, and steady-state kinetic parameters involved in phosphate formation for an enzyme. The benefits of using this methodology are that it is easy to use, inexpensive, easily scalable, and sample measurement requires only a spectrophotometer. While these assays are straightforward and highly reproducible they involve the quenching of the reactions, which denatures the protein of interest liberating any bound P_i. As such these assays are not able to differentiate between the formation of P_i during the reaction and the subsequent release of the phosphate from the enzyme (Fig. 2.1). Often the latter is delayed with respect to the chemical step and frequently serves important mechanistic functions (Lionne et al., 1995, Takagi et al., 2004, Savelsbergh et al., 2005, Wang et al., 2010). In addition the malachite green assay requires incubation steps in order to form the phosphate complexes that can be detected; meaning detection is not in real-time. Real-time detection of phosphate has applications in rapid-kinetics studies, for example, in the determination of the rates of phosphate release following a dephosphorylation step.

A related alternative to colorimetric assays is the use of radioisotope labels. The radioisotope approach to detection of phosphate utilizes substrates labeled with ^{32}P or ^{33}P. Protocols utilizing radioactive detection first involve incubation of a radiolabeled substrate with the enzyme studied, followed by chemical quenching of the reaction, and

subsequent detection of liberated radioactive phosphate (Craig et al., 2014). Detection of radioactive phosphate is usually achieved using liquid scintillation counting, or autoradiography (Craig et al., 2014). With liquid scintillation counting, a scintillation cocktail absorbs energy emitted by the radioisotope being detected and re-emits it as photons to be detected by a photomultiplier tube (Horrocks 1974). With autoradiography, modern methodology usually involves first resolving radioactive samples on a gel or thin-layer chromatography plate; followed by radioisotope detection using a phosphorimager screen (Craig et al., 2014). The phosphorimager screen can then be scanned with a laser, and light emissions detected (Craig et al., 2014). Similar to the colorimetric method, this type of methodology can be used to determine the steady-state kinetic parameters of phosphate formation by an enzyme (e.g. the Michaelis constant, or catalytic efficiency). For example, assays utilizing γ^{32}P labeled GTP have been used to determine the rates of enzymatic GTP hydrolysis by GTPases (De Laurentiis and Wieden 2015, Coatham et al., 2016). Although radioactive detection of phosphate is a useful tool, the main restriction in terms of running this type of assay is the availability of radioactively labeled substrate analogs. Additionally, this type of assay is not able to distinguish between phosphate formation and phosphate release. Information regarding the phosphate product release step is key to understanding complex enzyme mechanisms.

Although the aforementioned colorimetric and radioactive methods of phosphate detection are useful for researchers in detecting the enzymatic formation of phosphate, they lack the fundamental ability to separate the chemical step of phosphate formation from the step of phosphate release due the required quenching step, which will liberate any enzyme-bound phosphate. Phosphate release from a protein active site has a variety

of roles in biological systems; the release of phosphate by an enzyme can contribute substantially to the function and mechanism of an enzyme or system. For example, phosphate release from actin bound myosin·ADP·P_i triggers force generation in muscle fibers (Takagi et al., 2004). As well, some ATPases are rate-limited by the release of phosphate when performing ATP hydrolysis (Lionne et al., 1995, Wang et al., 2010). These and other examples have led to the hypothesis that phosphate release kinetics are key to a variety of biological processes (Brune et al., 1994) and that quenching based detection methods might miss the critical role this mechanistic step might play in an enzymes reaction mechanism.

2.1 Phosphate binding protein

To overcome these shortcomings a protein biosensor-based system to detect the release of the formed phosphate from the enzyme of interest has been developed (Brune et al., 1994). This method is able to dissect the chemical step of phosphate formation from the mechanistic step of phosphate release. The phosphate-binding protein method for phosphate detection utilizes a fluorescently labeled variant of *Escherichia coli* PhoS. *In vivo* PhoS is a component of the phosphate-specific transport (PST) system, which is the primary method for uptake of extracellular phosphate in *E. coli* (Hsieh and Wanner 2010). The PST system is comprised of an ATP-binding cassette (ABC) transporter protein, as well as high-affinity phosphate-binding proteins such as PhoS (Willsky and Malamy 1980, Goody 2013). Gene expression of PhoS is up-regulated by phosphate limitation, and the protein is synthesized with an N-terminal signal sequence which is cleaved upon localization to the periplasm (Magota et al., 1984).

Previous structural data suggests that PhoS undergoes a large conformational change upon phosphate binding (Hirshberg et al., 1998). PhoS consists of two-domains and a flexible hinge region, and binding of phosphate occurs at an interface between the respective N and C-terminal domains. In the phosphate-bound PhoS structure, the protein is "closed" and phosphate is completely desolvated and coordinated by enzyme residues via hydrogen bonds (Luecke and Quiocho 1990, Ledvina et al., 1996). In the phosphate-free PhoS structure, the protein adopts an open conformation providing easy access of the binding pocket to the bulk solvent.

Multiple mutations of PhoS have been developed in order to allow for labeling with thiol reactive probes and to detect the conformational change triggered by phosphate binding (Brune et al., 1994, Hirshberg et al., 1998). The most widely used version of PhoS for phosphate release assays is the A197C variant labeled with *N*-[2-(1-maleimidyl)ethyl]-7-(diethylamino)coumarin-3-carboxamide (MDCC). This variant provides ideal positioning for the MDCC fluorophore on the edge of the phosphate binding site in PhoS, which allows for a signal change of up to 5-fold upon phosphate binding (Hirshberg et al., 1998). Binding of phosphate to PhoS A197C-MDCC is rapid (1.36×10^8 M^{-1} s^{-1}), and tight ($K_D \sim 0.1\mu M$), making this system ideal for real-time detection of the release of free phosphate *in vitro* (Brune et al., 1994). This system has been successfully commercialized and ThermoFisher Scientific currently sells PhoS A197C-MDCC at a price of $450/10 nanomoles. As a comparison, the amount of MDCC fluorophore required to produce 10 nanomoles of PhoS A197C-MDCC would cost less than a dollar based on current prices.

As an alternative to this system another fluorescent labeling strategy of PhoS worth noting is double-tetramethylrhodamine (rho) labeled PhoS A17C I76G A197C. This labeled protein maintains rapid, tight binding of phosphate, has an additional mutation in the hinge-region of PhoS, and has been shown to produce a improved signal change of up to 18-fold (Okoh et al., 2006). In this variant, the distance of the rho dyes allows for the formation of a non-covalent, low-fluorescence rho dimer in the absence of phosphate. When phosphate binds to double-rho labeled PhoS A17C I76G A197C, the conformational change of PhoS reorients the dyes into their high-fluorescence monomer form. However, a reported issue with this construct is contamination with single-labeled rho-PhoS following the labeling reaction. Subsequent chromatographic steps are required in order to remove the highly fluorescent single-labeled rho-PhoS (Solscheid et al., 2015).

The very tight binding of phosphate to labeled PhoS makes it very useful for measuring phosphate concentrations in the low micromolar range. However at higher phosphate concentrations this system will be expensive to use as labeled PhoS will need to be in excess over phosphate. This is because, like the colorimetric and radioactive systems described in this literature review, phosphate detection is stoichiometric. In a recent PhoS paper, the authors introduced many variants of PhoS with affinities for phosphate ranging from <1 μM to >200 μM (Solscheid et al., 2015). The decreased affinity of these PhoS constructs allows for sub-stoichiometric quantities of labeled PhoS to be used for detecting phosphate, making this system useful for detecting high quantities of phosphate. However in situations where rapid, sensitive detection of phosphate is required the high-affinity PhoS constructs would be better suited.

In general, the reported protein production and purification procedures for PhoS are laborious. PhoS has been previously purified by first expressing from a plasmid, pSN5182 (Brune et al., 1994), in *E. coli* using its native promoter and signal sequence, followed by purification from the periplasm using osmotic shock, followed by ion-exchange chromatography, and size-exclusion chromatography (Brune et al., 1994). Recently, expression of PhoS variants from a pET22b plasmid using isopropyl β-D-1-thiogalactopyranoside (IPTG) induction has been reported (Solscheid et al., 2015) and purification was performed as previously described (Morita et al., 1983, Okoh et al., 2006, Solscheid et al., 2015). This demonstrated that PhoS variants could be expressed using an IPTG-inducible promoter, allowing for higher expression levels than previously described. For labeling of PhoS variants with rho or MDCC, various adjustments to standard protocols have been reported to increase product yield and labeling efficiency (Brune et al., 1994, Brune et al., 1998, Okoh et al., 2006). For example, some studies have aimed to improve labeling efficiency by removing phosphate contamination from PhoS variant protein preparations. The presence of phosphate can decrease labeling efficiency because in a phosphate-bound PhoS variant crystal structure, the 197C thiol is buried likely not accessible for labeling (Hirshberg et al., 1998). The methods for removing phosphate contamination include using an additional chromatographic step, or including a "phosphate mop" in the labeling reaction (Brune et al., 1994, Brune et al., 1998, Okoh et al., 2006). The phosphate mop utilizes 7-methylguanosine and purine nucleoside phosphorylase, which is able to remove free phosphate by its conversion to ribose 1-phosphate (Brune et al., 1994). Although these studies have succeeded in improving the protein expression and labeling efficiency, the main challenge is that many of these procedures remain inefficient. For example, little has been done to improve the

purification procedure of PhoS variants, and utilizing modern purification strategies may allow researchers to produce PhoS A197C-MDCC at a lower cost.

2.2 Objectives: Phosphate Detection

In short the PhoS system of phosphate detection is extremely useful, however its high price and laborious purification procedure may prevent it from being a cost-effective research tool. In this thesis, I present a simplified methodology of PhoS A197C-MDCC production that has drastically decreased the cost of producing this biosensor relative to a commercially available product. As well, I demonstrate that this methodology produces PhoS A197C-MDCC suitable for use in real-time phosphate release assays.

2.2 Chapter 2. Figures and Tables

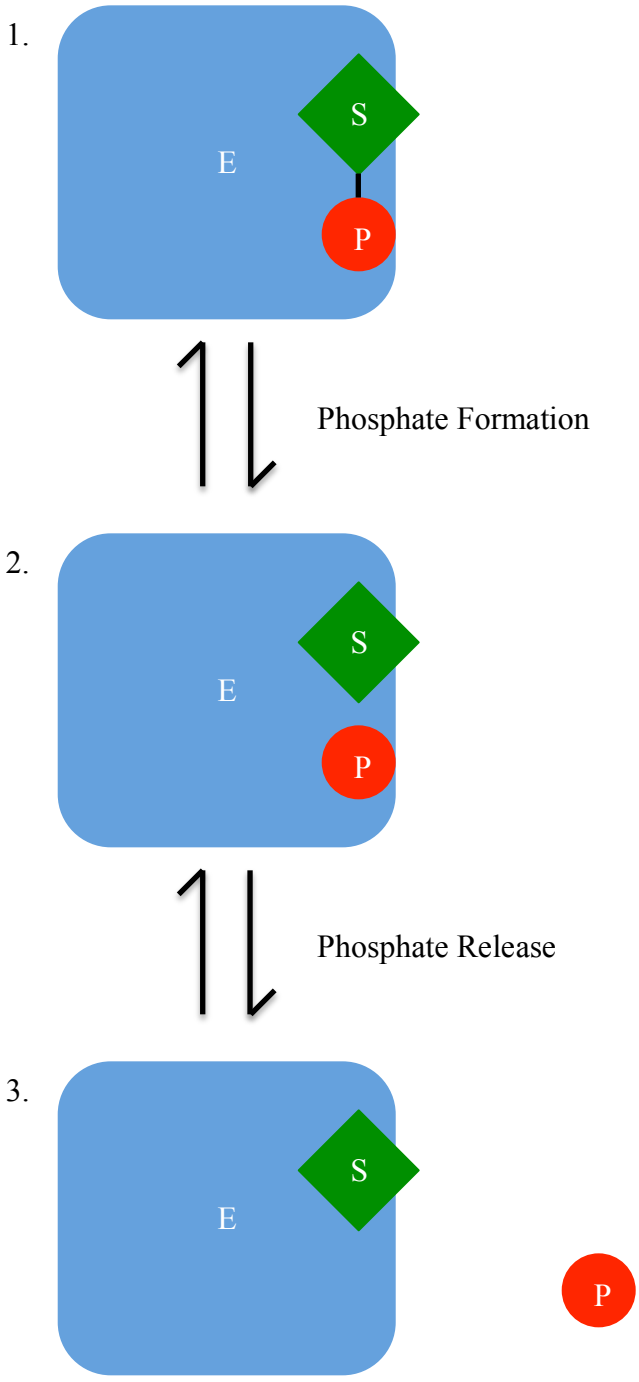

Figure 2.1. Schematic representation of an enzyme-catalyzed dephosphorylation reaction, distinguishing phosphate formation from phosphate release. In this hypothetical mechanism, an enzyme (E) is bound to a phosphorylated substrate (S-P) in Complex 1. The bond between the substrate (S) and the phosphate (P) is broken, resulting in Complex 2. Following this phosphate release occurs, resulting in free phosphate. In this figure an E-S complex is shown for Complex 3, and it should be noted that S could dissociate from the complex before, after, or at the same time as P.

Chapter 3: A kinetic study of quaternary structure formation and phytate binding by PhyA from *Selenomonas ruminantium*

3.1 Introduction

Myo-inositol polyphosphates (IPs) are ubiquitous in nature and have a variety of physiological roles. IPs chelate cations, and are the principal form of phosphate storage in plant seeds (Reddy et al., 1982). Additionally, IPs serve a variety of roles in cellular signalling events. For example, *myo*-inositol 1,2,3,4,5,6 – hexa*kis*phosphate (IP_6, or phytate) is involved in mRNA export, DNA repair, bacterial pathogenicity, RNA editing, plant development, and apoptosis (York et al., 1999, Hanakahi et al., 2000, Chatterjee et al., 2003, Macbeth et al., 2005, Tan et al., 2007, Majerus et al., 2008). Other IPs are involved in cell signalling processes as well; for example, *myo*-inositol 1,4,5-triphosphate is exemplary in terms of biological activity for its role as a second-messenger (Best et al., 2010).

Phytate-Degrading Enzymes (PDEs) are enzymes that dephosphorylate phytate, producing lower-order IPs. PDEs are generally referred to as phytases, and this class of enzymes is sub-divided into four groups: histidine acid phosphatases, β-propeller phytases, purple-acid phosphatases, and protein tyrosine phosphatase-like phytases (PTPLPs). Although these enzymes all share the ability to degrade IPs, their mechanisms of action, structural features, and substrate specificities differ. The PTPLP group of phytases contains a PTP domain and use a PTP-like mechanism to dephosphorylate IPs (Puhl et al., 2007). The significance of this evolutionary relationship between PTPLPs and PTPs is not well understood; however, the best studied-eukaryotic PTPs are

regulators of cellular function (Chen et al., 2015). The representative PTPLP PhyA from *Selenomonas ruminantium* (PhyAsr) contains this PTP domain, yet the protein shows little activity against conventional PTP substrates and contains various structural features that confer specificity to IPs (Chu et al., 2004, Puhl et al., 2007, Gruninger et al., 2012).

PhyAsr is able to dephosphorylate IPs in a stepwise fashion, releasing the IP product after each round of catalysis (Puhl et al., 2007). PhyAsr follows its primary dephosphorylation pathway for the conversion of IP_6 to *myo*-inositol 2-phosphate >80% of the time (Puhl et al., 2007). This type of selectivity for one substrate in the pathway over other very similar substrates is interesting from an enzyme engineering perspective. For example, knowledge of this selectivity by PhyAsr may lead to the ability to engineer a PTPLP to produce a specific IP. Production of a specific IP would be useful from an industrial prospective, as current methods to produce stereospecific IPs are costly. Knowledge of the kinetic mechanism of PhyAsr provides useful information in understanding the basis of IP selectivity by this enzyme. However, there is limited data describing the kinetic mechanism of PhyAsr. In previous publications, catalytically inactive (C252S) fluorescently labeled variants of PhyAsr have been developed to study substrate binding (Gruninger et al., 2012). This fluorescence reporter system utilizes amino acid substitution in PhyAsr that allow for labeling with a thiol reactive probe (either H188C or K301C substitution). The respective variants contain substitutions at a position near the IP binding site, and produce a detectable change in fluorescence upon IP binding. Previous data has suggested that: 1) the affinity of IP_6 to labeled PhyAsr H188C/C252S is below 1 micromolar, 2) binding of IP_6 to labeled PhyAsr H188C/C252S follows a mechanism with at least two steps and 3) that the Michaelis constant (K_M) value

is several orders of magnitude larger than the Equilibrium Dissociation constant (K_D), suggesting that it does not follow a Michaelis-Menten mechanism (Gruninger et al., 2012). Also it has been shown that phosphate is an inhibitor of PhyAsr catalyzed dephosphorylation of IP_6 to *myo*-inositol 1,2,4,5,6 – pentakisphosphate (IP_5) under multiple-turnover conditions (Gruninger et al., 2012). However, only little is known regarding the molecular mechanism of substrate binding to PhyAsr, and the kinetic details for PhyAsr-catalyzed dephosphorylation of IPs are largely missing.

An additional feature of PhyAsr that has remained mostly unexplored is the mechanistic role of PhyAsr dimerization, which has been observed in crystal structures (Fig. 3.1) as well as size-exclusion chromatography purification procedures (Gruninger 2009). This observation raises a number of questions. For example, at what protein concentration does PhyAsr dimerize, and at what rate does PhyAsr dimerization occur? Is PhyAsr dimerization physiologically relevant? If so, what role does the formation of this quaternary structure serve *in vivo*? Systematic dissection of the fluorescence signal observed with the previously reported fluorescently labeled mutations of PhyAsr (Gruninger et al., 2012) reveal that it is sensitive to dimerization, meaning these constructs are useful to studies of the kinetics of PhyAsr dimerization.

Here, I report for the first time the K_D, minimal molecular mechanism, and respective rate constants of PhyAsr dimerization using a fluorescence reporter assay using the stopped-flow technique. As well, I describe IP_6 binding to dimerized PhyAsr both in the presence, and absence of phosphate.

3.2 Methods and Materials

Protein Overexpression and Purification

Escherichia coli BL21 (DE3) cells (Novagen) containing the previously constructed pET28b::PhyAsr constructs (Puhl et al., 2007, Gruninger et al., 2012) were used as an inoculum in LB medium with kanamycin (50 μg/mL) and incubated overnight (37°C, 200 RPM). The following day, fresh LB medium with kanamycin was inoculated with the overnight culture (2% v/v). The resulting culture was grown to an OD_{600} of 0.6, and induced with isopropyl-β-D-thiogalactopyranoside to a final concentration of 1 mM. Cells were harvested approximately 3 h later by centrifugation (5000 × g, 5 minutes, 4°C), flash frozen, and stored at -80°C.

Cells were resuspended in 7 mL Buffer A (20 mM KH_2PO_4 (pH 7.0), 300 mM NaCl, 1 mM β-mercaptoethanol (BME), 15 mM imidazole) per gram of cells. The suspension was sonicated (Branson Sonifier 450, Danbury, CT) on ice for 1 min at 60% duty cycle (repeated twice, with a 5 minute break between cycles), cell debris was removed by centrifugation (5000 × g, 5 minutes, 4°C), and the supernatant was centrifuged again (30 000 × g, 30 minutes, 4°C). The supernatant was loaded onto a Ni^{2+} immobilized metal affinity chromatography (IMAC) resin (Bio-Rad, Hercules, CA) column that was equilibrated with Buffer A on a low-pressure liquid chromatography system (Bio-Rad BioLogic LP) at a flow rate of 1.5 mL/min. The column was then washed with Buffer A until A_{280} of flow-through decreased below 0.2 absorbance units. Protein was eluted using Buffer E (Buffer A with 400 mM imidazole). Fractions were analyzed for purity using sodium dodecyl sulfate polyacrylamide gel electrophoresis

(SDS-PAGE) stained with Coomassie Brilliant Blue, and fractions containing PhyAsr were pooled and dialyzed into Equilibration Buffer (20 mM Tris (pH 8.0), 100 mM NaCl, 1 mM βME) for labeling.

Fluorescent Labeling

For every 400 nmoles of protein, 5 mL of Ni^{2+} IMAC resin (Bio-Rad) equilibrated in 40 mL equilibration buffer was used for batch binding. The resin was centrifuged (all centrifugation steps in this fluorescent labeling protocol were 500 × g, 5 minutes, 20°C), and buffer solution decanted. Resin was washed with 1 volume of Labeling Buffer (20 mM Tris (pH 8.0), 100 mM NaCl, 10% glycerol). Following centrifugation, the buffer solution was decanted. The wash step was repeated 8 times and the resin containing bound PhyAsr was resuspended in 1 volume of Labeling Buffer, and a 20-fold molar excess of 5-iodoacetamidofluorescein (5-IAF; Thermo Fisher Scientific, Waltham MA) was added (from a freshly made 30 mM stock in dimethylformamine). The resin was then incubated overnight at 30°C with shaking (240 RPM, Innova 4080 incubator shaker, New Brunswick Scientific, Enfield, CT). The reaction was stopped by washing with 1 volume of Labeling Buffer, the supernatant was decanted, and the wash repeated until the supernatant solution appeared colourless. Elution of labeled protein was performed with 1 volume of Elution Buffer (Labeling Buffer with 500 mM imidazole) until elution appeared colourless. Fractions collected were examined via SDS-PAGE under UV light, and fractions containing labeled PhyAsr were pooled and dialyzed into 2 L of 20 mM sodium acetate buffer (pH 5.0), 300 mM NaCl (4 exchanges at 4°C, dialysis tubing: Spectra/Por molecular weight cut-off 6-8 kDa). Labeling efficiencies were typically

~70%, and were determined using spectrophotometry and manufacturer's labeling formulae (Equations 3.1 and 3.2, ThermoFisher).

$$[c] = (A_{280} - (A_{491} \times 0.3)) / \varepsilon_p \times L \quad (3.1)$$

$$\text{Labeling efficiency (\%)} = (A_{491} / (\varepsilon_d \times [c] \times L)) \times 100\% \quad (3.2)$$

Where [c] is the protein concentration (M), A_{280} is the absorbance at 280 nm of the labeled protein preparation, A_{491} is the absorbance at 491 nm of the labeled protein preparation, 0.3 is a correction factor which adjusts for the absorbance that fluorescein will have at 280 nm, ε_p is the molar extinction coefficient of the protein (80 330 M^{-1} cm^{-1}), L is the spectrophotometer path length (cm), and ε_d is the molar extinction coefficient of the 5-IAF dye (82 000 M^{-1} cm^{-1}).

Data Analysis: Error Propagation

When indicated, standard deviation values were propagated using the equations below. For operations involving subtraction of one value with standard deviation from another, Equation 3.3 was used. For operations involving division or multiplication of values with standard deviation, Equation 3.4 was used.

$$d_c = \sqrt{((d_a)^2 + (d_b)^2)} \quad (3.3)$$

$$d_c / c = \sqrt{((d_a / a)^2 + (d_b / b)^2)} \quad (3.4)$$

Where d_a and d_b, are standard deviations associated with the mean values a and b respectively, and d_c is the error propagated standard deviation of the calculated value c.

Equilibrium Fluorescence Measurements

Fluorescence spectrophotometry experiments were conducted using a Quanta Master 60 Fluorescence Spectrometer (Photon Technology International, Edison, New Jersey; excitation wavelength: 488 nm, emission wavelength: 505 - 540 nm, excitation slit widths: 2 nm, emission slit widths: 4 nm, step size: 1 nm, integration: 1 s). All equilibrium fluorescence measurements were performed in 20 mM sodium acetate buffer (pH 5.0), 300 mM NaCl at 20°C. Experimental (IP_6 solution; n = 3) and control (Buffer Solution; n = 3) titrations were performed. The mean values obtained from the control were subtracted from the mean values of the experimental treatments, the absolute value of this calculation was plotted and standard deviation was propagated to produce error bars (Equation 3.3). Data was plotted using GraphPad Prism v. 5.0, and fit using a hyperbolic function (Equation 3.5). Equation parameters were as follows: B_{max} is maximum binding in the same units as Y, K_D is the dissociation constant, in the same units as X.

$$Y = B_{max} * X / (K_D + X) \quad (3.5)$$

Rapid Kinetics Measurements

Rapid kinetics measurements were performed in a KinTek SF-2004 apparatus using an excitation wavelength of 488 nm, and fluorescence emission was detected through 505 nm long-pass filters (NewPort, Irvine, CA). Experiments were performed in 20 mM sodium acetate buffer (pH 5.0), 300 mM NaCl at 20°C. Individual traces were fit using TableCurve exponential fitting (SigmaPlot). Fluorescence time courses obtained in the stopped-flow titration of labeled PhyAsr C252S/K301C with unlabeled PhyAsr

C252S/K301C (Fig. 3.4) were fit with either a one-exponential function (Equation 3.6), or a two-exponential function (Equation 3.7). Traces used in the stopped-flow titration of labeled PhyAsr H188C/C252S with IP_6 (Fig. 3.7) were fit with a two-exponential plus slope function (Equation 3.8), or a three-exponential plus slope function (Equation 3.9). Experimental traces testing the effect of 10 mM phosphate on IP_6 binding to PhyAsr H188C/C252S (Fig. 3.8) were fit with a three-exponential plus slope function (Equation 3.9). Equation parameters were as follows, fluorescence (F) observed at time *t*, final fluorescence (F_∞), A was signal amplitude with rate k_{app}, and m was slope.

One-exponential function:

$$F = F_\infty + A_1 * \exp(-k_{app1}t) \quad (3.6)$$

Two-exponential function:

$$F = F_\infty + A_1 * \exp(-k_{app1}t) + A_2 * \exp(-k_{app2}t) \quad (3.7)$$

Two-exponential function plus slope:

$$F = F_\infty + A_1 * \exp(-k_{app1}t) + A_2 * \exp(-k_{app2}t) + mt \quad (3.8)$$

Three-exponential function plus slope:

$$F = F_\infty + A_1 * \exp(-k_{app1}t) + A_2 * \exp(-k_{app2}t) + A_3 * \exp(-k_{app3}t) + mt \quad (3.9)$$

Data analysis was performed using GraphPad Prism v. 5.0. a hyperbolic function was used for fitting of amplitude data (Equation 3.5), and apparent rate plots were fit with a linear function (Equation 3.10).

$$k_{app} = [c] * k_1 + k_{-1} \quad (3.10)$$

Where k_{app} was the apparent rate observed at concentration [c], k_1 was the rate constant of the forward reaction, and k_{-1} was an approximation of the rate constant of the reverse reaction.

3.3 Results

Dimerization of PhyAsr. The mechanistic details of formation of PhyAsr quaternary structure are not well understood. To determine the K_D, and association rate constants of dimer formation, a fluorescence-based rapid kinetics experiment was performed using a stopped-flow apparatus. By mixing fluorescently labeled PhyAsr C252S/K301C with unlabeled PhyAsr C252S/K301C, an increase in fluorescence was observed (Fig. 3.2). The obtained time courses were best fit with a one-exponential (Equation 3.6), suggesting a one-step binding mechanism (Fig. 3.3A). Interestingly, at higher (≥ 1 μM protein concentration) a two-exponential function (Equation 3.7) best described the fluorescence change as function of time, indicating an additional step during formation of the PhyAsr dimer (Fig 3.3B). After performing this experiment at various protein concentrations, signal amplitudes and apparent rates obtained from the exponential fits were plotted as a function of protein concentration (Fig. 3.4), and analyzed to determine kinetic parameters (Table 3.1). A plot of signal amplitude of the first phase was plotted as a function of protein concentration and fit with a hyperbolic function (Equation 3.5) to yield a K_D of 1.6 ± 0.9 μM (Fig. 3.4A). A plot of signal amplitude of the second phase was plotted as a function of protein concentration and fit with a hyperbolic function (Equation 3.5) to yield a K_D of 1.0 ± 0.4 μM (Fig. 3.4C). The analysis of the concentration dependence of the two obtained apparent rate constants reveals that the k_{app1} describes the initial concentration dependent step of a two-step

binding mechanism (Fig. 3.4B). Consistent with a first-order structural rearrangement following initial complex formation, k_{app2} is concentration independent (Fig. 3.4D). The obtained plots of apparent rate as a function of protein concentration can be fit with a linear function (Equation 3.10) to determine $k_{1\ (\text{dimerization})}$, $k_{-1\ (\text{protein dissociation})}$, and $k_{2\ (\text{dimerization})}$ (Fig. 3.4, B and D). Using these parameters, $k_{-2\ (\text{protein dissociation})}$ was calculated using the formula $K_D = (k_{-1} \times k_{-2}) / (k_1 \times k_2)$. In summary, dimerization of PhyAsr involves at least two steps, proceeds slowly ($k_{1\ (\text{dimerization})} = 0.024 \pm 0.006\ \mu M^{-1}s^{-1}$, $k_{2\ (\text{dimerization})} = 0.0120 \pm 0.0009\ s^{-1}$), and has a K_D of approximately 1 μM.

Binding of IP_6 to dimerized PhyAsr. Previous work performed at 1 μM PhyAsr has estimated the affinity of monomeric PhyAsr to IP_6 to be in the sub-micromolar range (Gruninger et al., 2012). More recent work performed at 20 nM PhyAsr has estimated the affinity of monomeric PhyAsr to IP_6 to be approximately 90 nM (Steven Mosimann, personal communication). On this background I wanted to know if the dimerization of PhyAsr alters the binding affinity for IP_6. In order to investigate the binding of IP_6 to dimerized PhyAsr, the PhyAsr dimer experiments were performed at a protein concentration of 3 μM which is approximately 3 times above the K_D determined in the previous protein dimerization assay (Fig. 3.4, Table 3.1). At 3 μM PhyAsr over 75% of the protein will be exist as dimer (Equation 3.5). Using these conditions an equilibrium fluorescence titration of IP_6 was performed to determine K_D of IP_6 for PhyAsr dimer. Upon binding of the IP_6 to PhyAsr and consistent with previous work (Gruninger et al., 2012), a decrease in fluorescein fluorescence was observed. The experiments were performed with two different fluorescently labeled variants; revealing that IP_6 binding to the two dimerized PhyAsr mutants occurs with similar affinity (C252S/K301C: $K_D = 46 \pm$

7 μM, H188C/C252S: K_D = 29 ± 7 μM) (Fig. 3.5). Interestingly, these K_D values are approximately 300-fold higher than the previously K_D of 90 nM for the binding of IP_6 to monomeric PhyAsr at a lower protein concentration. This suggests that dimerizaton of the PhyAsr modulates its substrate affinity.

Rapid kinetic studies of IP_6 binding to dimerized PhyAsr. To further investigate the kinetic mechanism of IP_6 binding to PhyAsr dimers, a rapid-kinetics analysis using the stopped-flow technique was performed to investigate the molecular mechanism and to obtain the rate constants describing this mechanism. Labeled PhyAsr H188C/C252S was used at a final concentration after mixing of 3 μM to preform the dimer and minimize the effect of protein dilution on the signal. The protein was rapidly mixed with various concentrations of IP_6. After mixing, a fluorescence decrease was observed consistent with the equilibrium titration. The resulting fluorescence time courses were best fit with either a two-exponential plus slope function (Equation 3.8), or a three-exponential plus slope function (Equation 3.9), depending on the concentration of IP_6 (Fig. 3.6). After performing this experiment at various IP_6 concentrations, signal amplitudes and apparent rates were plotted as a function of IP_6 concentration (Fig. 3.7) and fit to obtain the respective kinetic parameters summarized in (Table 3.2). In summary, binding of IP_6 to dimerized PhyAsr involved at least three steps. And the K_D obtained from this stopped-flow experiment was 21 ± 3 μM, a result within error of the K_D determined in the equilibrium fluorescence titration (*vide supra*) using the same mutant (H188C/C252S, Table 3.2).

IP_6 binding to dimerized PhyAsr in the presence of phosphate. It has been previously reported that PhyAsr catalyzed dephosphorylation of IP_6 to IP_5 is significantly hindered by the presence of 10 mM phosphate (Gruninger et al., 2012), although the K_D of phosphate binding to PhyAsr is not known. Little is known about the mechanistic details of this inhibition. For example, does phosphate prevent binding of IP_6 to PhyAsr under these conditions? Or does phosphate inhibit any of the steps previously observed in the stopped-flow assay? As a tool to study the impact of phosphate on the binding of IP_6 to PhyAsr, the aforementioned stopped-flow assay that mixed dimerized PhyAsr H188C/C252S with IP_6 was utilized. For this experiment a single concentration of IP_6 was tested, the assay was performed in the presence of 10 mM phosphate, and the results were interpreted by fitting the signal change data (Fig. 3.8). Under these experimental conditions, phosphate was at 10 mM concentration, which was previously shown to be inhibitory to PhyAsr up to an IP_6 concentration of 50 mM (Gruninger et al., 2012). To determine the impact of phosphate on IP_6 binding by PhyAsr, fit parameters in the presence or absence of phosphate were compared (Table 3.3). Results showed that there was little variance between fit parameters when comparing IP_6 binding to PhyAsr in the presence or absence of 10 mM phosphate. More specifically, the presence of phosphate did not affect any of the apparent rates; and only slightly affected two of the amplitude parameters. This result suggests that none of the kinetic parameters determined in this experiment were strongly inhibited by the presence of 10 mM phosphate. Meaning that phosphate does not affect IP_6 binding to dimerized PhyAsr, and inhibition likely occurs on another step not observed in this study.

3.4 Discussion

Little is known about the kinetic mechanism of how PhyAsr is able to select for different, consecutive IP substrates in its dephosphorylation pathway. This property of PhyAsr is of great interest to bioengineering applications. To this end it is important to develop an experimental framework that will allow for the determination of these enzymatic properties, ultimately instructing the systematic enzyme engineering. In this study, the first kinetic information and minimal molecular mechanism for the model PTPLP PhyAsr is reported with respect to its self-association and binding to IP_6.

*Dimerization of PhyAs*r. The reported observations support a sequential model of dimer formation, where the steps observed occur in succession (Fig. 3.9). Only the apparent rate of the first step is concentration dependent (Fig. 3.4B) suggesting a bi-molecular event, such as two PhyAsr proteins coming together to form a dimer. The apparent rate of the second step in the kinetic mechanism is not dependent on protein concentration (Fig. 3.4D) suggesting it is an event that occurs with one molecular entity, such as a conformational change of the enzyme that follows binding. This event likely occurs in proximity to the binding pocket given the location of the fluorescence reporter. In terms of the affinity of PhyAsr dimer formation, all methods used to determine the K_D produced values of approximately 1 - 2 μM (Table 3.1). The similarity between the amplitude versus protein concentration plots (Fig. 3.4, A and C) suggests that the first and second steps in dimer formation are coupled processes. For example, if 50% of the protein is binding and forming a dimer in step one, only that 50% subpopulation may undergo the post-binding conformational change.

With a K_D value of approximately 1 μM, it is possible that PhyAsr exists as a dimer *in vivo*. The cellular concentration of PhyAsr is not currently known, and the protein has previously been shown to localize to the outer surface of *S. ruminantium* (D'Silva et al., 2000). Signal peptide prediction software (Petersen et al., 2011) suggests that PhyAsr contains a signal peptide. However, the mechanism of PhyAsr export from the cell is not known. Bacteria can utilize different means of transporting a protein outside of the cell. These methods include co-translational transport with periplasmic intermediates, or post-translational transport (Kostakioti et al., 2005). With either type of transport, PhyAsr could fold before being transported across the outer membrane of the cell. It is possible that when PhyAsr is produced in a bacterial cell it forms dimers, when the protein is exported from the cell it is diluted and forms monomers. This type of mechanism suggests that dimerization could function to regulate the activity of PhyAsr depending on its localization. Although the presence of IPs in the bacterial cell has not yet been confirmed, one could envision a reduced affinity for the dimer to its substrate might reflect a structural rearrangement of the substrate-binding pocket, consistent with the observed second step in the kinetic mechanism (Fig 3.4D), to prevent "rogue" interactions with substrates inside of the cell or the periplasm and that the enzyme is only fully active when monomeric. In addition to PhyAsr crystalizing as a dimer (Gruninger 2009), two other published PTPLPs have been shown to exist as a dimer (Gruninger et al., 2009, Gruninger et al., 2014). However, the dimerization interface of these published structures and an additional unpublished PTPLP structure lacks conservation (Gruninger 2009, Steven Mosimann, personal communication). This observation suggests that either: 1) the property of dimerization modulating binding affinity for IP_6 is unique to PhyAsr, or 2) other PTPLPs are achieving similar means via different mechanisms.

Binding of IP_6 to dimerized PhyAsr. On this background it is interesting to investigate if dimerization has indeed the potential to modulate the affinity of PhyAsr to its substrate. Both PhyAsr mutants yielded similar K_D values for IP_6 binding (H188C/C252S, 29 ± 7 μM, and C252S/K301C, 46 ± 7 μM), which demonstrated that the labeling position does not influence the interaction of PhyAsr with substrate (Fig. 3.5).

Interestingly, cellular concentrations of IP_6 have been reported to range from 10-100 μM in eukaryotes (Best et al., 2010), the reported K_D values of ~35 μM fall within this range and thus could be physiologically relevant, as IP_6 binding to PhyAsr will be highly concentration dependent. At the low end of the concentration range essentially no IP_6 will be bound and at 100 μM IP_6 over 75% will be bound. A previous study has suggested that the K_D of 1 μM PhyAsr for IP_6 is in the low micromolar range (Gruninger et al., 2012). As well, unpublished data has estimated that the K_D for IP_6 is approximately 90 nM at 20 nM PhyAsr (Steven Mosimann, personal communication). The data presented in my current study was collected at a much higher protein concentration than what has been used previously. An explanation for this difference in K_D values is that quaternary structure of PhyAsr indeed modulates binding affinity to IP_6; and altering protein concentration could tune enzyme activity. One could argue that another possible explanation of this data is that the K_D determined in this study is for IP_6 binding to a different part of the binding pocket, which might be directed by the interactions formed between the two PhyAsr molecules in the dimer (e.g. occlusion of the high affinity binding site). The active site of PhyAsr contains a large electropositive cleft (Gruninger et al., 2012), therefore it may be the case that under high IP_6 concentrations the substrate binds to locations in the binding pocket other than the high affinity site. For example,

previously reported crystal structures of PhyAsr (protein databank 3MOZ and 1U25) each show ligand bound in a non-catalytically competent manner. In an effort to gain further insight into what was being observed in this binding assay, a rapid kinetics approach to studying IP_6 binding was utilized.

Rapid kinetic studies of IP_6 binding to dimerized PhyAsr. The rapid kinetics data collected suggests that IP_6 binds to PhyAsr via a very complex mechanism with at least three steps. This data is consistent with the wide range of substrates observed in previous studies (Puhl et al., 2007), in that IP_6 could be sampling multiple conformations in the PhyAsr binding site. As it has also been suggested that PhyAsr contains multiple, overlapping IP binding sites in the binding pocket (Gruninger et al., 2012). However, one can envision the remodelling of the PhyAsr binding site upon dimerization adding to the diversity of the binding site properties. This reorientation of the binding site could occlude the high-affinity binding site, or remodel the rates of conversion between the different states, thereby leading to an altered affinity.

Analysis of this rapid kinetics data set revealed a single IP_6 concentration-dependent step (Fig. 3.7B). This phase of the signal is likely an initial binding event. Because only one of these IP_6 concentration-dependent plots was observed, this provides evidence against the interpretation that binding of IP_6 to multiple areas of PhyAsr with varying affinities was occurring. For this dataset, the best model to represent this data is a sequential model rather than a parallel model (Fig. 3.9). This data displays a single concentration-dependent step (Fig. 3.7B) followed by two additional steps. For clarity,

the rate constants obtained have been summarized in a model of the kinetic mechanism of PhyAsr (Fig. 3.10).

The Apparent Rate 2 (k_{app2}) versus IP_6 concentration plot (Fig. 3.7D) appeared to represent a concentration independent step. However, the apparent rates appeared to decrease slightly as IP_6 concentration increased (Fig. 3.7D). For this figure the downward trend may be an artefact of fitting, as many data points may be reflective of multiple events. For instance, a third phase was fit for the three highest IP_6 concentration that were not distinguishable from the second phase for the lower IP_6 concentration treatments. For all concentrations tested below that concentration threshold, the molecular events of the second and third phase would be combined and displayed as a single data point in Fig 3.7D. One might argue that the downward trend observed (Fig. 3.7D) could be a result of substrate inhibition slowing down this second step as IP_6 accumulates. It has been previously shown that high concentrations of IP_6 can slow PhyAsr catalyzed dephosphorylation of IP_6 (Steven Mosimann, personal communication). It could be the case that when high concentrations of IP_6 are present the second step is slowed, resulting in the downward trend observed (Fig. 3.7D). However this is not strong evidence for the presence of substrate inhibition, if substrate inhibition was being observed one would expect to observe an additional binding (IP_6 concentration dependent) apparent rate in the stopped-flow analysis. That said, because PhyAsr utilizes a "ping-pong" reaction mechanism substrate inhibition could occur on subsequent binding steps not examined in my research. But in the context of my data, the second step (Fig. 3.7D) likely reflects a conformational change. More specifically, it could be a conformational change of the protein, or reorientation of the IP_6 substrate. Based on the data, the third phase of this

signal could also be a protein conformational change or substrate reorientation. This third phase requires a very high concentration of IP_6 in order to be detectable (Fig. 3.7F), which suggests it may not be a process that occurs *in vivo*. For the slope in these fits (m parameter, Equations 3.8 and 3.9), the values fit were likely photobleaching over the time-course of the experiment. To my knowledge, this is the first report describing detailed rapid-kinetics data of substrate binding to a PTPLP.

IP_6 binding to dimerized PhyAsr in the presence of phosphate. It has been reported that conversion of IP_6 to IP_5 by 1 μM PhyAsr is inhibited by the presence of 10 mM phosphate (Gruninger et al., 2012), however the specific step in the kinetic mechanism that was inhibited by phosphate remains unknown. The results reported in this study suggest that the presence of 10 mM phosphate had no major affect on any of the steps observed for IP_6 binding to PhyAsr (Table 3.3). From the work conducted in this study, it is clear that the apparent rates of substrate binding for each step observed are not altered (Table 3.3), however, the amplitude of the first and third phases decreased by approximately two-fold. However, the observed phosphate inhibition effect in the multiple-turnover activity likely occurs on a step other than the steps reported by the fluorescent label and that is subsequent to binding of the substrate. For example, phosphate could prevents proper orientation of IP_6 immediately prior to catalysis. Alternatively, because the used reporter system gives similar output for IP_6 binding to PhyAsr in the presence or absence of phosphate, one could argue that the reporter is unable to distinguish between IP_6 binding in a catalytically competent versus catalytically incompetent manner. To address this concern, different labeling positions could be utilized with the goal of distinguishing between catalytically competent versus

catalytically incompetent binding. For example, a labeling strategy that positions a fluorophore reaching into the P-loop of PhyAsr may accomplish this. However, in this study phosphate did not have a major effect on any of the steps observed using this IP_6 binding stopped-flow assay. And more research is required in order to determine what specific kinetic steps of PhyAsr catalyzed IP_6 dephosphorylation are inhibited by phosphate.

Conclusions and future directions. This study has described for the first time the kinetic parameters of PhyAsr dimerization, and rapid kinetic studies of IP_6 binding to dimers of a PTPLP. The PhyAsr dimer forms with a K_D of approximately 1 μM, and the role of dimerization is not yet known. The binding of IP_6 to the PhyAsr dimer was found to have a lower affinity than previously described for IP_6 binding to lower concentrations of PhyAsr. This result suggests that dimerization could modulate PhyAsr binding affinity for IP_6. PhyAsr is exported from the cell, so one could envision dimerization acting as a switch to alter the enzyme properties inside the cell versus outside of the cell. Additionally, I show that the presence of phosphate had no major effect on any phase of IP_6 binding to PhyAsr observed in this study. Future studies should further explore the kinetic mechanism of PhyAsr by determining kinetic parameters for other IPs binding to PhyAsr in monomer and dimer form. As well, these studies should utilize alternative methods to confirm the K_D values reported in this study. This would be useful to validate the assumption that the fluorescein dye does not alter the dimerization or IP_6 binding properties of PhyAsr. For example, isothermal titration calorimetry could be performed to determine the binding properties of unlabeled PhyAsr. Future studies should also

investigate the nature of phosphate inhibition on PhyAsr, and address what step in the kinetic mechanism is inhibited by phosphate.

3.5 Chapter 3. Figures and Tables

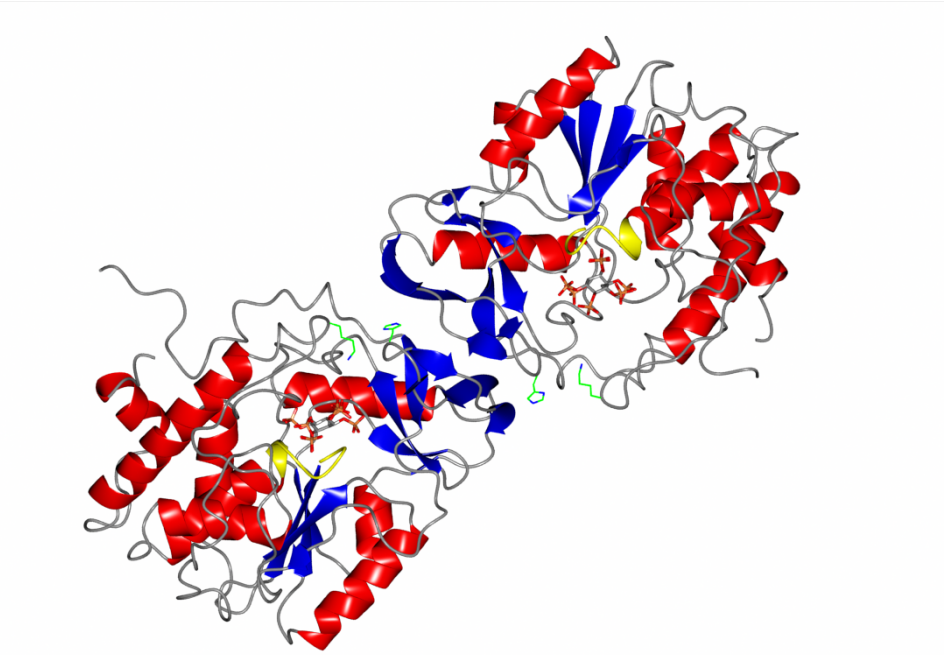

Figure 3.1. Cartoon representation of dimerized PhyAsr C252S in complex with IP_6. Alpha helices are shown in red, beta sheets are shown in blue, and the P-loop is shown in yellow. The side chains of H188 and K301 are shown in green, and these positions have previously been mutated to cysteine to allow for labeling with thiol reactive probes for fluorescence studies. PDB ID: 3MMJ.

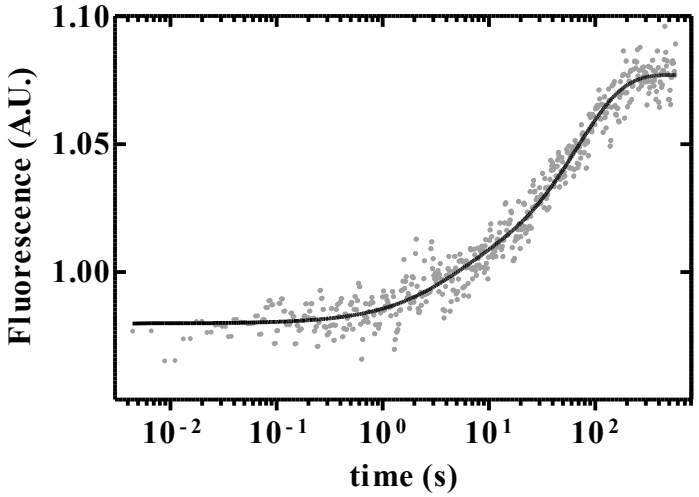

Figure 3.2. Dimerization of labeled PhyAsr produces a fluorescence signal increase. Pre-steady state kinetics of labeled PhyAsr C252S/K301C (500 nM) binding to unlabeled PhyAsr C252S/K301C (7.5 μM). Raw data from a representative stopped-flow time course (grey dots) was fit with a two-exponential function (black line). A.U., arbitrary units.

A.

B.

Figure. 3.3. A schematic representation of a one-step (A), and two-step (B) binding model (B). In both schematics, A and B are molecular entities that bind to form a complex (AB, or a different conformation of AB, AB*).

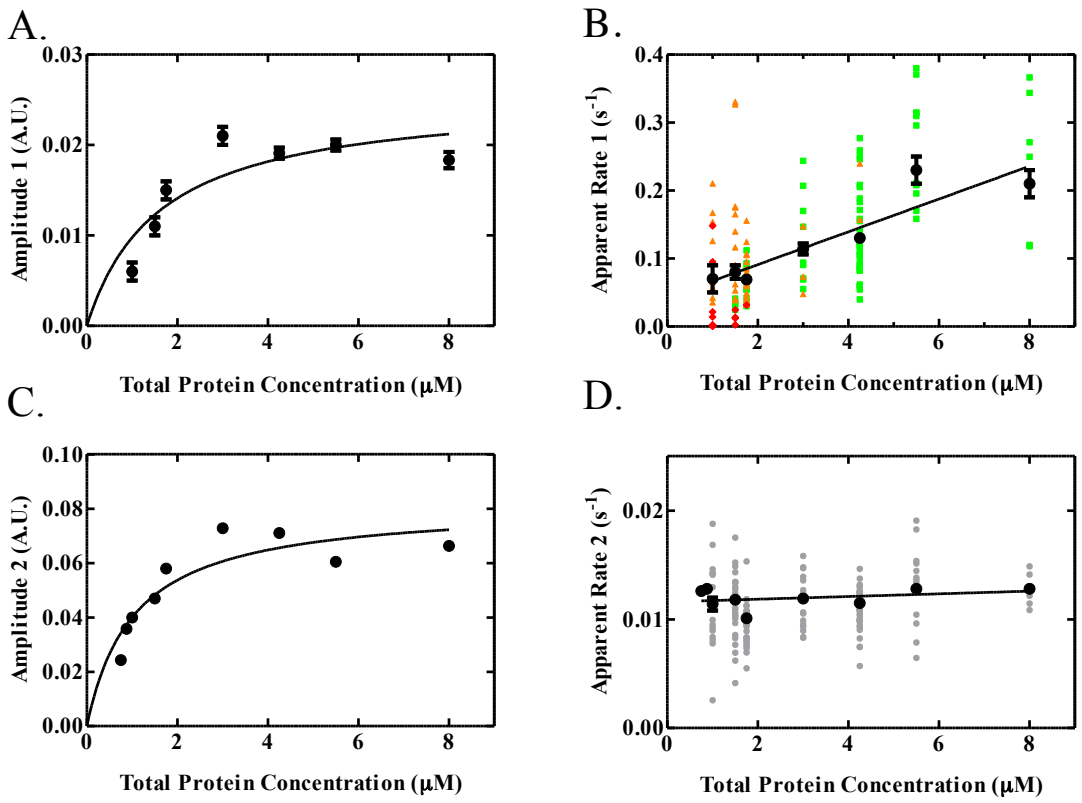

Figure 3.4. Dimerization of PhyAsr follows a mechanism of at least two resolvable steps. Signal amplitudes and apparent rates of PhyAsr C252S/K301C dimer formation are plotted. Black dots indicate values obtained by fitting the average trace for each treatment; error bars reflect 95% confidence interval of the fit. Amplitude plots of the first phase (A), and the second phase (C) were fit with a hyperbolic function (Equation 3.5, R^2 values were 0.74 and 0.81 respectively). Apparent rate plots of the first phase (B), and the second phase (D) were fit with a linear function (Equation 3.10). In (B), coloured data points are from individual traces and colour indicates the error of the fit (95% confidence interval), bins were assigned as follows; green squares, error was less than 35% of the value of the data point reported, orange triangles, error was greater than 35% but less than 100% of the value of the data point reported, red diamonds, error was greater than 100% of the value of the data point reported. In (D), grey data points are from individual traces. For each treatment, the number of shots was ≥ 5, and the cuvette concentration of labeled PhyAsr was 500 nM. The kinetic parameters determined from this experiment are listed in Table 3.1.

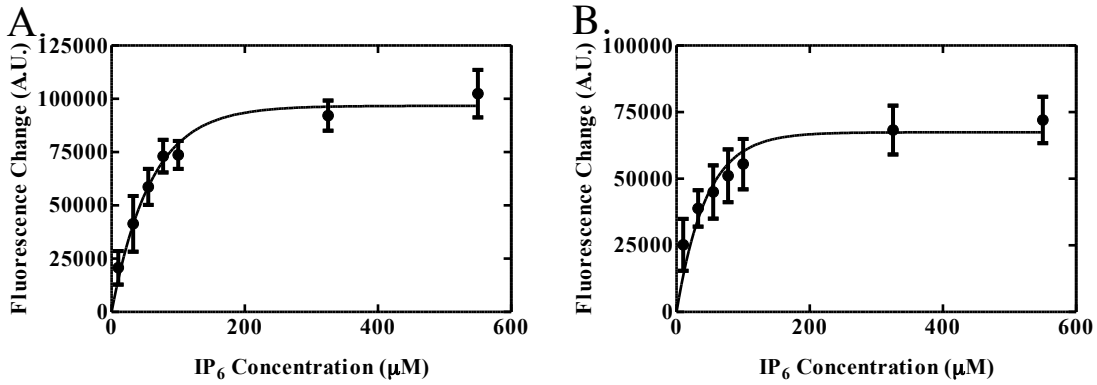

Figure 3.5. Binding of IP_6 to dimerized PhyAsr occurs with similar affinity regardless of labeling position. Peak fluorescence (λ = 512 nm) from an emission scan of dimerized, labeled PhyAsr C252S/K301C (A) or H188C/C252S (B) at various concentrations of IP_6. Sample fluorescence was measured using fluorescence spectrophotometry, and plots were both fit with a hyperbolic function (Equation 3.5, R^2 values were 0.92 and 0.77 respectively). For both titrations fluorescence values were corrected by using a control titration with buffer (methods), and the concentration of PhyAsr was 3 μM (n = 3, mean ± s.d.)

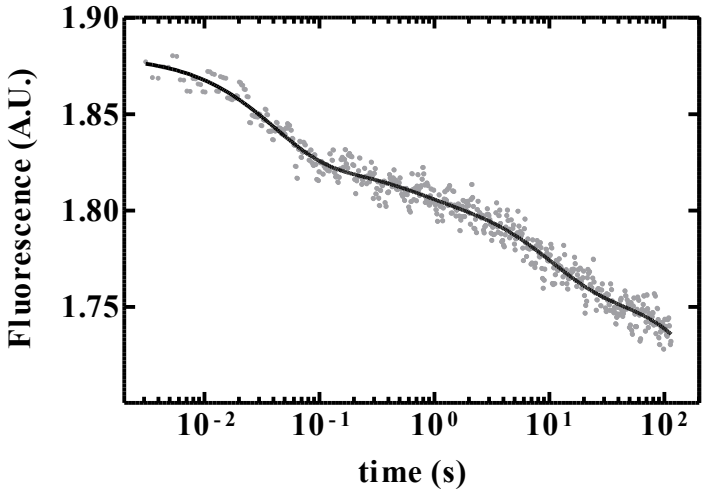

Figure 3.6. Binding IP_6 to dimerized PhyAsr produces a fluorescence signal decrease with multiple steps. Pre-steady state kinetics of IP_6 binding to dimerized PhyAsr H188C/C252S. Raw data from a representative stopped-flow time course (grey dots) was fit with a three-exponential plus slope function (black line; see methods section, Equation 3.7). A.U., arbitrary units.

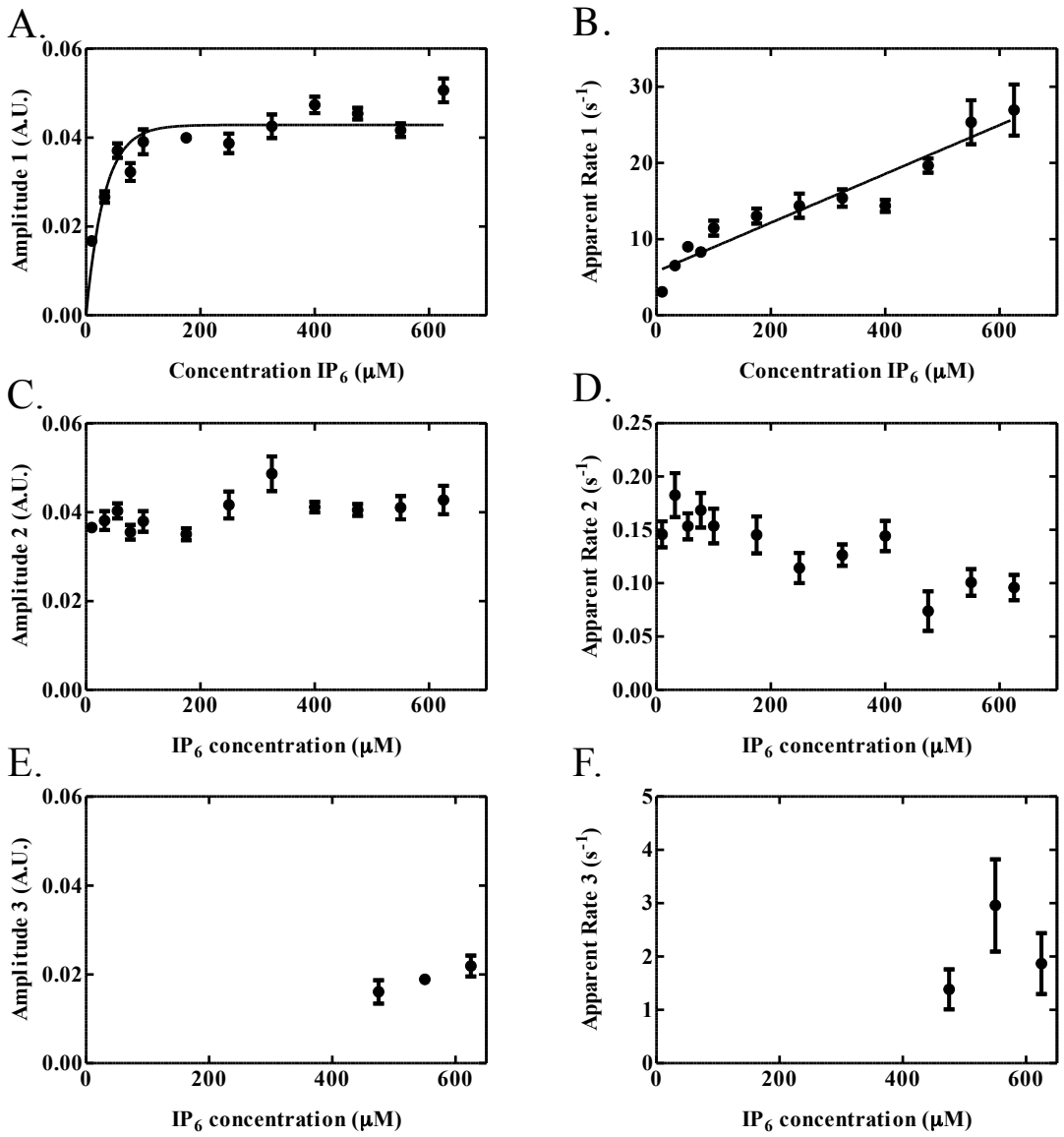

Figure 3.7. Binding of IP_6 to dimerized PhyAsr includes multiple, resolvable steps. Rapid kinetics analysis of IP_6 binding to dimerized, labeled PhyAsr H188C/C252S. Traces were fit with a two exponential function, or a three exponential function when [IP_6] was greater than 450 μM. Amplitude for the first phase (A) is plotted against IP_6 concentration and fit with a hyperbolic function (Equation 5, R^2 value was 0.71). Apparent rate of the first phase (B) is plotted against IP_6 concentration and fit with a linear function. Amplitudes of the second (C), and third (E) phases are plotted but not fit. Apparent rates of the second (D), and third (F) phases are plotted but not fit. All kinetic parameters determined from this figure are listed in Table 3.2. Concentration of PhyAsr H188C/C252S was 3 μM, and data points shown reflect the mean ± s.d. of the individual fits, n = 6.

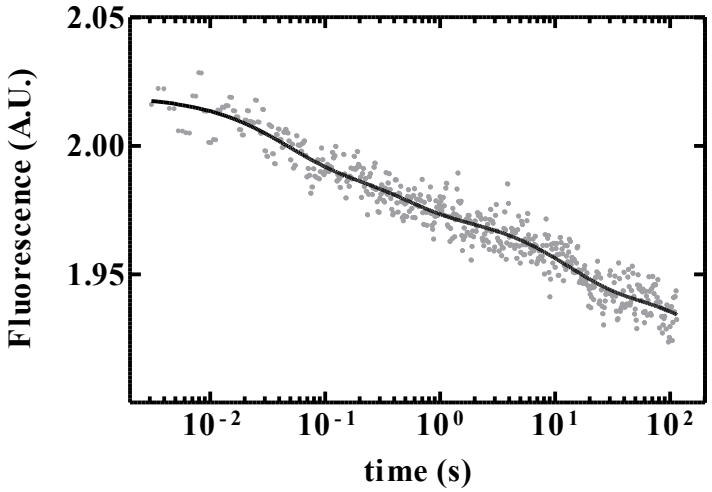

Figure 3.8. Binding of IP_6 to dimerized PhyAsr is detectable in the presence of 10 mM phosphate. Pre-steady state kinetics of IP_6 binding to dimerized PhyAsr H188C/C252S in the presence of 10 mM phosphate. Raw data from a representative stopped-flow time course (grey dots) was fit with a three-exponential plus slope function (black line; see methods section, Equation 3.7). A.U., arbitrary units.

A.

B.

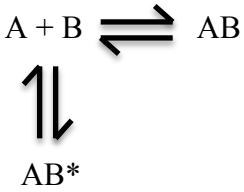

Figure. 3.9. A schematic representation of a sequential binding model (A), and a parallel binding model (B). In both schematics, A and B are molecular entities that bind to form a complex (AB, or a different conformation of AB, AB*).

A.

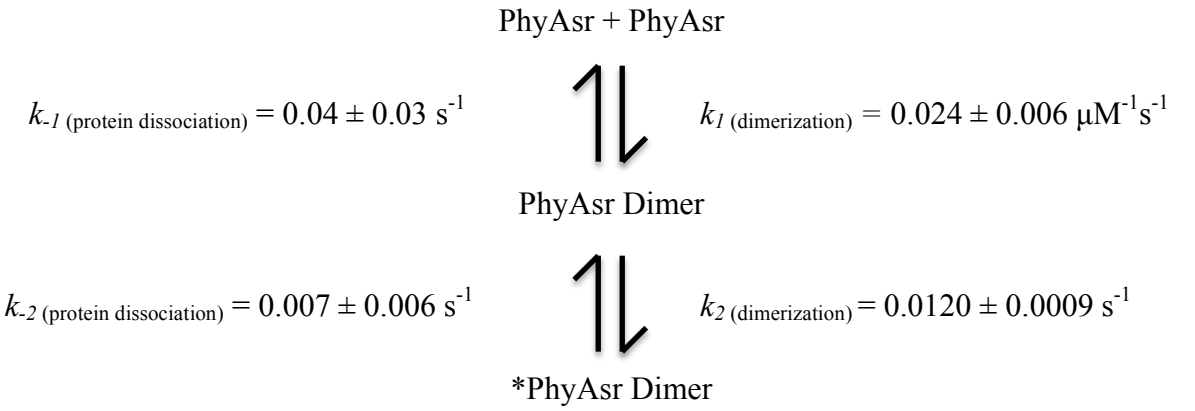

B.

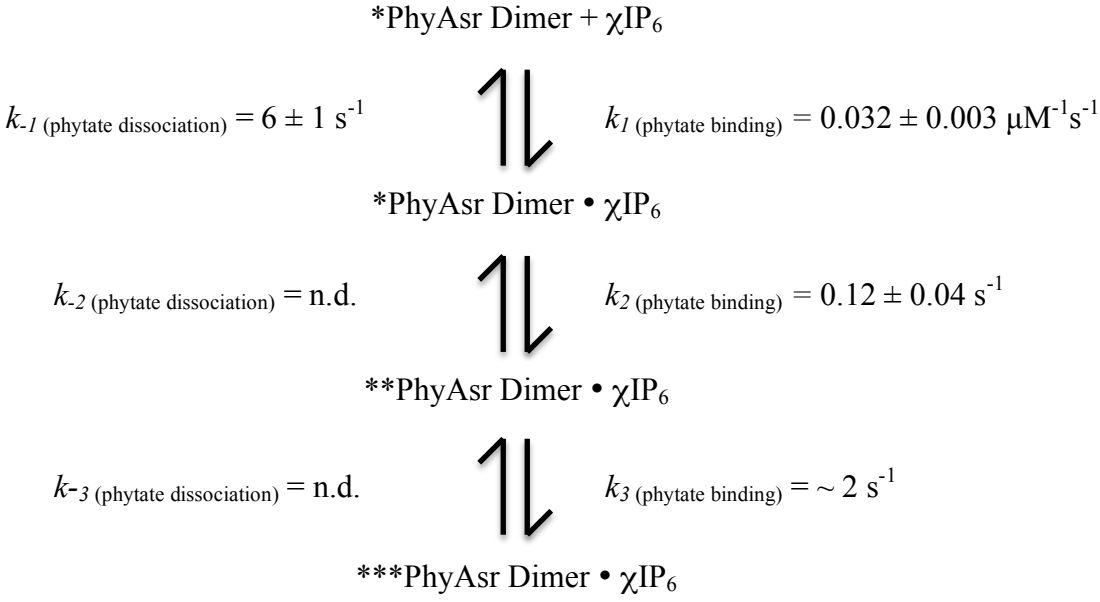

Figure 3.10. Minimal kinetic mechanism of PhyAsr dimer formation (A), and IP_6 binding to PhyAsr dimers (B). In (A) PhyAsr monomers bind to form a dimer, and undergo a conformational change producing *PhyAsr dimer. In (B), there is an IP_6 binding event to preformed *PhyAsr dimer which may then undergo a series of conformational changes. n.d., not determined.

Table 3.1. Summary of dissociation constants and rate constants for the dimerization of PhyAsr.

Constant	Value
K_D (± s.d., μM)	1.6 ± 0.9[a]
K_D (± s.d., μM)	1.0 ± 0.4[b]
k_1 (± s.d., $\mu M^{-1}s^{-1}$)	0.024 ± 0.006[c]
k_2 (± s.d., s^{-1})	0.0120 ± 0.0009[d]
k_{-1} (± s.d., s^{-1})	0.04 ± 0.03[e]
k_{-2} (± s.d., s^{-1})	0.007 ± 0.006[f]

[a] Determined from fitting data in Fig. 3.4A with Equation 3.5
[b] Determined from fitting data in Fig. 3.4C with Equation 3.5
[c] Determined from slope of fit in Fig. 3.4B with Equation 3.10
[d] Determined from the mean and standard deviation of all treatments in Fig. 3.4D
[e] Determined from the y-intercept of fit in Fig. 3.4B with Equation 3.10
[f] Calculated using the equation $K_D = (k_{-1} \times k_{-2}) / (k_1 \times k_2)$, solving for k_{-2} and using 1.0 ± 0.4 μM for K_D, error propagated using Equation 3.4

Table 3.2. Summary of dissociation constants and rate constants for the binding of phytate to dimerized PhyAsr.

Constant	Value
K_D (± s.d., μM)	46 ± 7[a]
K_D (± s.d., μM)	29 ± 7[b]
K_D (± s.d., μM)	21 ± 3[c]
k_1 (± s.d., $\mu M^{-1}s^{-1}$)	0.032 ± 0.003[d]
k_2 (± s.d., s^{-1})	0.12 ± 0.04[e]
k_3 (± s.d., s^{-1})	~2[f]
k_{-1} (± s.d., s^{-1})	6 ± 1[g]
k_{-2}	n.d.
k_{-3}	n.d.

[a] Determined from fitting data in Fig. 3.5A with Equation 3.5
[b] Determined from fitting data in Fig. 3.5B with Equation 3.5
[c] Determined from fitting data in Fig. 3.7A with Equation 3.5
[d] Determined from slope of fit in Fig. 3.7B with Equation 3.10
[e] Determined from the mean and standard deviation of all treatments in Fig. 3.7D
[f] Estimated from Fig. 3.7F
[g] Determined from y-intercept of fit in Fig. 3.7B with Equation 3.10
n.d., not determined

Table 3.3: Fit parameter comparison for PhyAsr binding IP_6 in the presence, or absence of phosphate. Representative traces from each data set are shown with their fits in Figures 3.5, and 3.7. Equation syntax is as described in the methods section (Equation 3.7). Values reflect the mean of best-fit parameters ± s.d. (n = 6).

	A_1 (A.U.)	k_1 (s^{-1})	A_2 (A.U.)	k_2 (s^{-1})	A_3 (A.U.)	k_3 (s^{-1})	m (A.U./s)
No added Pi	0.051 ± 0.007	27 ± 8	0.022 ± 0.006	1.9 ± 1.4	0.043 ± 0.008	0.10 ± 0.03	-0.00020 ± 0.00009
+ 10 mM Pi	0.022 ± 0.006	25 ± 13	0.022 ± 0.001	1.8 ± 0.4	0.021 ± 0.006	0.11 ± 0.05	-0.00013 ± 0.00008

Chapter 4: Streamlined production of a fluorescently labeled *Escherichia coli* phosphate binding protein (PhoS) suitable for rapid-kinetics applications.

4.1 Introduction

Inorganic phosphate (P_i) is ubiquitous in nature and plays a variety of roles in biological systems. The binding and release of P_i in an enzyme active site can contribute substantially to enzyme function. For example, P_i release from actin bound myosin·ADP·P_i triggers force generation in muscle fibers (Geeves and Holmes 2005). In many ATPases multiple-turnover ATP hydrolysis is rate-limited by the release of P_i (Trentham et al., 1972, Brune et al., 1994, Lionne et al., 1995, Wang et al., 2010). These and other examples demonstrate that P_i release kinetics are key to a wide range of biological processes.

Previously developed methods to assay P_i release kinetics utilize *E. coli* phosphate-binding protein (PhoS). *In vivo* PhoS is a high-affinity binding protein involved in active transport of P_i, and gene expression is induced by P_i starvation (Magota et al., 1984). Expression of PhoS has been achieved from a construct containing *phoS* in the plasmid pSN5182 in *E. coli* ANCC75 cells using its native promoter and N-terminal signal sequence (pre-*phoS*) (Brune et al., 1994, Brune et al., 1998). The N-terminal signal sequence of pre-PhoS is cleaved upon localization to the periplasm, producing mature PhoS (Morita et al., 1983). Exploiting this localization for purification, protocols have been developed which selectively rupture the outer cell membrane, allowing for the

purification of periplasm-localized proteins from a low P_i environment (Willsky and Malamy 1980, Magota et al., 1984).

Structural studies indicate that P_i binding occurs at an interface between the N and C terminal domains of PhoS, where binding stabilizes a large conformational change (Hirshberg et al., 1998). To enable real-time P_i-release assays based on the rapid binding of the released P_i to PhoS, Brune and coworkers developed a N-[2-(1-maleimidyl)ethyl]-7-(diethylamino)-coumarin-3-carboxamide (MDCC) labeled PhoS A197C (Brune et al., 1994). The labeling of PhoS at C197 positions MDCC on the edge of the P_i binding site and results in up to a 5-fold increase in fluorescence upon P_i binding (Brune et al., 1994). PhoS A197C-MDCC binds P_i tightly ($K_D \sim 0.1\mu M$) and rapidly (1.36×10^8 M^{-1} s^{-1}) making this system a sensitive method for detecting rapid changes in P_i concentration *in vitro* (Brune et al., 1994). However, the expression and purification of PhoS using this system is laborious due to the low expression of the native promoter and the isolation form the periplasm. The commercially available version of PhoS A197C-MDCC retails at a cost of $2809 (CAD) for 100 nanomoles (ThermoFisher P/N PV4407).

Therefore, the primary objective of this work was to develop a simplified, efficient, and cost-effective methodology to produce PhoS A197C-MDCC suitable for use in rapid-kinetics applications measuring P_i release. Currently PhoS purification procedures involve localization of the protein to the periplasm, followed by purification from the periplasm, requiring multiple chromatographic steps to obtain pure protein. In

order to improve upon this purification procedure, it is critical to test if the localization to the periplasm is critical for the function of the PhoS A197C-MDCC as well if the purification could be simplified by using affinity chromatography. To this end two expression vectors were designed and the resulting PhoS A197C-MDCC was characterized regarding its suitability for rapid-kinetics approaches and benchmarked against the commercially available Phosphate Sensor. These expression vectors included (1) *phoS* A197C without signal sequence in pET28b and (2) *phoS,* A197C in pET22b, utilizing the N-terminal pET22b signal sequence for periplasmic localization. Both constructs included a C-terminal His-tag, which allowes for simple batch purification using Ni^{2+} affinity chromatography.

To assess the utility of rapid-kinetic approaches such as the stopped-flow technique, my PhoS A197C-MDCC preparation was tested in a real-time P_i release assay. For this, P_i release following GTP hydrolysis by LepA/EF4 bound to the 70S ribosome was measured. The translational GTPase LepA/EF4 has been proposed to be involved in back-translocation of the ribosome, where LepA/EF4 recognizes a defective translocation reaction and gives EF-G a second chance to translocate the tRNAs correctly (Qin et al., 2006). Recent studies have shown that the structural dynamics of the C-terminal domain of LepA/EF4 strongly influences its multiple turnover GTPase activity (De Laurentiis and Wieden 2015). The P_i release kinetics of LepA/EF4 remains unknown, and knowledge of P_i release kinetics from this enzyme may be useful in deciphering key enzyme features, as well as its kinetic mechanism.

4.2 Materials and Methods

PhoS A197C expression construct design

The coding sequence for *E. coli* K12 *phoS*, including the mutation for A197C (Genbank coding sequence NC_000913.3, 3910485 - 3911525 complement, protein accession number NP_418184.1), was synthesized (Bio Basic Inc.) without its native promoter or N-terminal signal sequence (25 amino acid N-terminal deletion). This construct had flanking *Nco*I/*Xho*I sites, and was inserted into pET28b (pET28b::*phoS* A197C), and pET22b (pET22b::*phoS* A197C). Upon expression the resulting proteins both had a C-terminal His-tag fusion, and the protein produced from the pET22b construct contained an N-terminal signal sequence for periplasmic localization.

Overexpression of PhoS A197C from pET28b::*phoS* A197C *in E. coli BL21 (DE3)*

A flask containing 500 mL LB broth (supplemented with 40 μg/mL kanamycin) was inoculated with an overnight culture to $OD_{600} \approx 0.1$ and incubated at 37°C with shaking at 200 RPM. At a culture $OD_{600} \approx 0.6$, isopropyl β-D-1-thiogalactopyranoside (IPTG) was added to a final concentration of 1 mM. The culture was incubated overnight, and cells were harvested by centrifugation (10,000 × g, 10 min, 4°C) at a final culture OD_{600} of 4.55. Cells were flash frozen in liquid nitrogen and stored at -80°C prior to cell lysis.

Cell lysis: Sonication method used on cells containing pET28b::*phoS* A197C

Cells were resuspended in 7 mL of Buffer A (50 mM Tris-Cl (pH 7.5 at 4°C), 1 mM $MgCl_2$, 300 mM NaCl, 10 mM imidazole, 15% v/v glycerol, 5 mM β-mercaptoethanol, 1 mM phenylmethylsulfonylfluoride (PMSF)) per gram of cells. Lysozyme was added at a final concentration of 1 mg/mL and cell suspension incubated at 4°C with repeated inversion for 30 min. Subsequently, this mixture was sonicated (Branson Sonifier 450, Danbury, CT) on ice for 1 min at 60% duty cycle (repeated twice, with a 5 minute break between cycles) and the insoluble fraction containing cell debris was collected by centrifugation (30 000 x g, 15 min, 4°C). The supernatant was transferred to a new tube, flash frozen, and stored at -80°C.

Overexpression of A197C pre-phoS from pET22b::*phoS* A197C

An overnight culture of *E. coli* BL21(DE3) cells containing the pET22b::*phoS* A197C plasmid construct was diluted 1:50 in LB broth containing 100 mg/L ampicillin and grown 12 hours at 37°C. An aliquot of this culture was diluted 1:50 in 500 mL Minimal medium A (120 mM Tris·HCl (pH: 7.2), 80 mM NaCl, 20 mM KCl, 20 mM NH_4Cl, 3 mM Na_2SO_4, 640 µM KH_2PO_4, 200 µM $MgSO_4$, 200 µM $CaCl_2$, 10 µM $FeSO_4$, 2 g/L glucose, 100 mg/L ampicillin, and 10 mg/L thiamine) and grown for 16-20 hours prior to centrifugation (10,000 × g, 15 min, RT). Pelleted cells were resuspended in 500 mL Minimal medium B (Minimal medium A, except 64 µM KH_2PO_4) and grown for 12-16 hours to a final culture OD_{600} of 3.87, and harvested by centrifugation (10,000 × g, 15

min, RT). Cells were subjected to the osmotic shock procedure immediately after harvesting.

Osmotic shock of cells containing pET22b::phoS A197C protein product

PhoS A197C was isolated from the periplasm of *E. coli* using a previously reported osmotic shock procedure (Willsky and Malamy 1980). Harvested cells were washed with 40 mL Buffer B (30 mM NaCl, 10 mM Tris-HCl (pH 7.5)) per gram of cells and centrifuged (5000 × g, 10 min, 4°C). The cell pellet was washed again with Buffer B, and resuspended in 40 mL of 33 mM Tris-HCl (pH 7.5) per gram of cells. One volume of Stage I buffer (40% sucrose, 33 mM Tris-HCl (pH 7.5), 100 µM ethylenediaminetetraacetic acid (EDTA)) was added with rapid mixing prior to a ten minute incubation at room temperature. Cells were pelleted by centrifugation (13,000 × g, 10 min, 4°C) and the supernatant decanted. The pellet was rapidly dispersed in 80 mL Stage II buffer (500 µM $MgCl_2$) per gram of cells and incubated on a rotary shaker (180 RPM, 10 min, 4°C). The resulting suspension (shockate) was centrifuged (13,000 × g, 10 min, 4°C), and the supernatant containing the released periplasmic enzymes was flash frozen and stored at -80°C.

Purification of PhoS A197C

Cell lysate or osmotic shockate was thawed and applied to a Ni^{2+} IMAC resin (BioRad) column prewashed with Buffer A on a LPLC (BioRad BioLogic LP) at a flow

rate of 1.5 mL/min. The column was washed with Buffer A until the absorbance at 280 nm of flow-through decreased below 0.2 A.U. protein was eluted using Buffer C (Buffer A with 250 mM imidazole). The collected fractions were analysed by sodium dodecyl sulfate polyacrylamide gel electrophoresis (SDS-PAGE) and fractions containing PhoS A197C were pooled and dialyzed into Buffer D (20 mM Tris-HCl pH 8.0, 100 mM NaCl, 10 mM imidazole) for labeling. All preparations of PhoS A197C were determined to have a purity of >95% based on ImageJ densitometry analysis of an SDS-PAGE gel stained with Coomassie Brilliant Blue.

Fluorescent labeling of PhoS A197C with MDCC

This procedure was used for all protein preparations, independent of the expression construct. PhoS A197C (100 μM concentration in labeling reaction, 15 mL labeling reaction volume), was batch-bound to 3.5 mL Ni^{2+} IMAC resin (BioRad) in Labeling Buffer (20 mM Tris pH 8.0, 100 mM NaCl, 10 mM imidazole). Next, five-fold molar excess MDCC (Sigma P/N 05019, 500 μM concentration in the 15 mL labeling reaction; From a freshly prepared 25 mM stock in dimethylformamide) was added dropwise to the mixture, and the labeling reaction was incubated in an end-over-end mixer for 5 hours at RT, then at 4°C for 10 hours. The resin was collected by centrifugation (1000 × g, 2 min, RT), and the supernatant was decanted, followed by six washes with 2.5 resin volumes of Labeling Buffer (1000 × g, 2 min, RT). Elutions were performed with 2 resin volumes of Elution Buffer (Labeling Buffer with 500 mM imidazole). Samples from the labeling procedure were analyzed by SDS PAGE, unstained gels were first examined under UV light to confirm the presence of the label then re-

examined after staining with Coomassie Brilliant Blue. Elutions containing PhoS A197C-MDCC were pooled and dialyzed into Storage Buffer (10 mM Tris pH 7.6, 50 mM NaCl, 10 mL sample into 2 L buffer, 4 changes, dialysis tubing: spectra pore molecular weight cut-off 6-8 kDa). The protein yield from the labeling procedure was ~70%, and labeling efficiencies ranged from 60% to >90%. PhoS A197C-MDCC concentration, and labeling efficiencies were determined using spectrophotometry as previously described (Equations 4.1-4.3, (Brune et al., 1994)). The following equation parameters were used: 0.164 was a correction factor accounting for MDCC absorption at 280 nm (Brune et al., 1994), ε_{280}PhoS was 61880 M^{-1} cm^{-1} and determined by ExPASy ProtParam using primary sequence data (Gasteiger et al., 2005) L was instrument path length in cm, ε_{430}MDCC was 46800 M^{-1} cm^{-1} (Brune et al., 1994).

PhoS A197C Concentration: $(A_{280} - (A_{430} * 0.164)) / \varepsilon_{280}\text{PhoS} * L$ (4.1)

MDCC Concentration: $A_{430} / \varepsilon_{430}\text{MDCC} * L$ (4.2)

Labeling Efficiency: (Equation 4.2 / Equation 4.1) * 100% (4.3)

Equilibrium Fluorescence Measurements

Fluorescence spectrophotometry experiments were conducted using a Quanta Master 60 Fluorescence Spectrometer (Photon Technology International; excitation wavelength: 420 nm, emission wavelength: 425 – 622 nm, excitation slit widths: 1 nm, emission slit widths: 2 nm, step size: 1 nm, integration: 1 s). All equilibrium binding measurements were performed in 10 mM Tris (pH 7.6), 50 mM NaCl at 20°C. Data was plotted using GraphPad Prism v. 5.0.

Rapid-Kinetics Measurements

Rapid kinetics experiments were performed in a KinTek SF-2004 rapid mixing device (stopped-flow) using an excitation wavelength of 420 nm, and fluorescence emission was detected through 450 nm long-pass filters (NewPort). Before each experiment, the stopped-flow syringes and cuvette were incubated with the "P_i mop" system for 10 minutes to remove residual P_i (Brune et al., 1994). The P_i mop consisted of 0.5 U/mL purine nucleoside phosphorylase (Sigma P/N N8264), and 200 μM 7-methylguanosine (Sigma P/N M0627). Experiments in the stopped-flow were performed in $TAKM_7$ Buffer (50 mM Tris pH 7.5, 30 mM NH_4Cl, 70 mM KCl, 7 mM $MgCl_2$). Individual traces were fit using TableCurve (Sigmaplot) exponential fitting using a one-exponential function (Equation 4.4), or a three-exponential function (Equation 4.5)

One-exponential function:

$$F = F_\infty + A_1 * \exp(-k_{app1}t) \quad (4.4)$$

Three-exponential function:

$$F = F_\infty + A_1 * \exp(-k_{app1}t) + A_2 * \exp(-k_{app2}t) + A_3 * \exp(-k_{app3}t) \quad (4.5)$$

Where F was the fluorescence observed at time *t*, final fluorescence was F_∞ and A was signal amplitude with rate k_{app}.

Cloning, expression, and purification of components to test P_i *release from 70S-stimulated LepA/EF4 GTP hydrolysis*

LepA/EF4 was previously cloned into pET28a using the NdeI and HindIII restriction sites, expressed in *E. coli* BL21(DE3) cells, and purified as previously

described (De Laurentiis and Wieden 2015). Ribosomes were purified from 50 g of *E. coli* MRE600 cells as previously described (Milon et al., 2007, Shields et al., 2009). GTP was purchased from Sigma Aldrich, and purified away from GDP as previously described (Wilden et al., 2006).

4.3 Results

Impact of PhoS localization – To compare if purification of PhoS from cytosol or from the periplasm affects labeling efficiency PhoS A197C was expressed from both pET22b::*phoS* A197C and pET28b::*phoS* A197C, followed by purification and labeling with MDCC. In the case of the pET22b::*phoS* A197C the included signal sequence localizes the expressed protein to the periplasm. It is unclear how important the periplasmic location or the osmotic shock procedure are to yield PhoS A197C that can efficiently be labeled, which was previously suggested to be due to a lower P_i contamination in the resulting protein (Brune et al., 1998). For the pET28b::*phoS* A197C, the expression and cell-lysis conditions were much less laborious; however, it is unclear if these conditions would yield sufficiently pure protein that can be efficiently labeled and that retains its activity for phosphate detection.

To compare the performance of the respective fluorescently labeled proteins, the achievable increase in MDCC fluorescence upon addition of inorganic phosphate was determined (Fig. 4.1A). Results revealed a fluorescence increase of 1.6-fold, or 1.7-fold at the MDCC emission maxima upon addition of excess P_i to PhoS A197C-MDCC obtained form the respective expression system. Under similar conditions the Phosphate sensor (ThermoFisher P/N PV4406) showed a 2.4-fold fluorescence increase (Fig. 4.1B). This

clearly shows that purification of PhoS from the cytosol via His-tag purification is a viable alternative to other published protocols (Brune et al., 1994, Brune et al., 1998, Okoh et al., 2006, Solscheid et al., 2015). Therefore, further characterisation was only conducted using the pET28b::*phoS* A197C protein derived and compared to the Phosphate sensor from ThermoFisher.

Rapid-kinetics measurements *of P_i binding to PhoS A197C-MDCC.* In order to examine the kinetics of P_i binding to my PhoS A197C-MDCC preparation and the commercially available Phosphate Sensor, the stopped-flow technique was used. Mixing of PhoS A197C-MDCC or Phosphate Sensor with P_i resulted in a exponential fluorescent increase consistent with previous reports (Brune et al., 1994, Brune et al., 1998) and that could be best fit with a one-exponential equation (Fig. 4.2). In order to obtain kinetic parameters, a P_i-titration was performed for both proteins. The results of this experiment showed that my PhoS A197C-MDCC preparation, and the ThermoFisher Phosphate Sensor yielded the same value for the rate constant of P_i binding (k_{on} = 33 ± 2 $\mu M^{-1} s^{-1}$ and k_{on} = 34 ± 7 $\mu M^{-1} s^{-1}$ respectively). This further demonstrates that my PhoS A197C-MDCC system is able to preserve the kinetic properties of the commercially available system (Fig. 4.3). However, consistent with equilibrium data showing smaller florescence change upon P_i binding the amplitude of the signal change was larger for the Phosphate Sensor compared to my PhoS A197C-MDCC preparation (amplitudes were approximately 2.5 A.U. and approximately 1.75 A.U. respectively, Fig. 4.4). For both preparations, the amplitude of the signal change upon P_i binding was independent of P_i concentration (Fig. 4.4).

Rapid kinetics of P_i release from 70S-stimulated LepA/EF4 GTP hydrolysis. Understanding the rate of the P_i release in the mechanistic analysis of enzyme functions may reveal key enzyme features that are currently not understood. For example, previous research on another translational GTPase EF-G has shown that P_i release is controlled by interactions between the ribosomal protein L7/12 and EF-G, and interrupting these interactions strongly inhibited P_i release (Savelsbergh et al., 2005). However, P_i release from 70S ribosome-stimulated GTP hydrolysis by LepA/EF4 had not yet been studied. In order to assess if PhoS A197C-MDCC is suitable for this analysis P_i release from the LepA/EF4-GDP-Pi complex was measured using the stopped-flow approach previously used for EF-G (Savelsbergh et al., 2005). To this end LepA/EF4 (8 μM) was incubated with GTP (120 μM) to preform the LepA/EF4-GTP in one syringe at a concentration approximately five times above the previously reported K_D of 23 ± 11 μM (De Laurentiis and Wieden 2015). The contents of this syringe were then rapidly mixed with a solution of 70S ribosomes (2 μM) and PhoS A197C-MDCC (2.5 μM). Both solutions also contained 0.1 U/mL PNP, and 200 μM 7-methylguanosine as a P_i mop. The P_i mop was included in the experiment to remove residual phosphate from the reaction solutions prior to sample mixing. The removal of phosphate using the P_i mop occurs slowly (Brune et al., 1994), no interference of the P_i mop system with the detection of P_i release using PhoS A197C-MDCC was observed. The resulting fluorescence signal was best fit with a three-exponential function (Fig. 4.5) consistent with reports for EF-G and that reveal a rapid initial burst followed by a slower multiple turnover phase (Table 4.1).

4.4 Discussion

For the kinetic analysis of dephosphorylating enzymes using rapid kinetics approaches such as stopped-follow, the release of the formed P_i can be observed using fluorescently labeled variants of phosphate binding proteins. However, the use of the commercially available phosphate sensor is often cost prohibited. Furthermore, previous methods to purify PhoS are laborious, and expression was driven by its native promoter (Brune et al., 1994). The characterization of the His-tagged PhoSA197C reported here demonstrates that export of PhoS into the periplasmic space is not required for proper folding and function of PhoS A197C, as well as the respective fluorescence-based detection of P_i binding. Furthermore, I report for the first time the addition of a C-terminal His-tag to simplify the purification of the PhoS from the cytosol via Ni^{2+} affinity chromatography. PhoS A197C remains fully functional as a fusion protein. Consistent with previous work, PhoS A197C expression can be driven by an IPTG inducible promoter (Solscheid et al., 2015) to increase expression and avoid P_i starvation induced expression.

Binding of P_i to His-tagged PhoS A197C-MDCC is as rapid as P_i binding to the Phosphate Sensor (Fig. 4.3) and therefore suitable for the rapid detection of P_i. Similar to the equilibrium P_i binding experiments, stopped-flow characterization revealed an approximately two-fold larger signal-change for P_i binding to the Phosphate Sensor than to PhoS A197C-MDCC. Additionally, results suggest that binding of P_i is tight, as the fraction of P_i bound does not change between 4 – 7 μM P_i (Fig. 4.4). This suggests that all P_i concentrations tested are far above the K_D of both PhoS A197C-MDCC and Phosphate Sensor for P_i, which is consistent with previously reported data (Brune et al., 1994).

The His-tagged PhoS A197C-MDCC was used to characterise the P_i release-kinetics following 70S ribosome-stimulated GTP hydrolysis by LepA/EF4 (Fig. 4.5). The first phase ($27 \pm 9\ s^{-1}$) is likely the rate of P_i release following the first round of GTP hydrolysis. Interestingly, the apparent rate observed for the first phase is at the upper limit of what can be detected with my PhoS A197C-MDCC reporter system. Given a mixing chamber concentration of 1 μM 70S, the maximum concentration of P_i that can be produced after the first round of hydrolysis is 1 μM. At a P_i concentration of 1 μM, the rate for P_i biding to PhoS A197C-MDCC is 33 s^{-1}. Therefore, the apparent rate of 27 ± 9 s^{-1} for the first phase should likely be treated as a lower limit for the rate of P_i release in the burst phase. The second phase ($1.4 \pm 0.3\ s^{-1}$) likely reflects multiple turnover release of P_i. The multiple turnover phase is slower than the burst phase, as it requires turnover of LepA/EF4. This mechanism of a burst phase, followed by a multiple turnover phase has been previously observed with another translational GTPase, EF-Tu (Savelsbergh et al., 2005). The observed third phase was previously not described for P_i release from a ribosome-stimulated translational GTPase. There are several potential explanations for this additional phase. For example multiple subpopulations of LepA/EF4, or ribosomes in an experiment can cause P_i to be released at a different rate. More specifically preparations of 70S ribosomes often contain 50S contamination, and it could be this subpopulation of 50S ribosomes in the experiment that result in this additional phase. However, additional research will need to be completed to decipher the three-phase behaviour of P_i release from 70S-stimulated LepA/EF4 GTP hydrolysis to clearly understand this mechanism.

In summary - His-tagged PhoS A197C can be successfully purified using Ni^{2+} chromatography from the cytosol of *E. coli* and subsequently efficiently labeled with MDCC. This provides a simplified and robust methodology for production of labeled PhoS for research applications requiring large quantities of the protein to detect binding of P_i in real-time.

4.5 Chapter 4 Figures and Tables

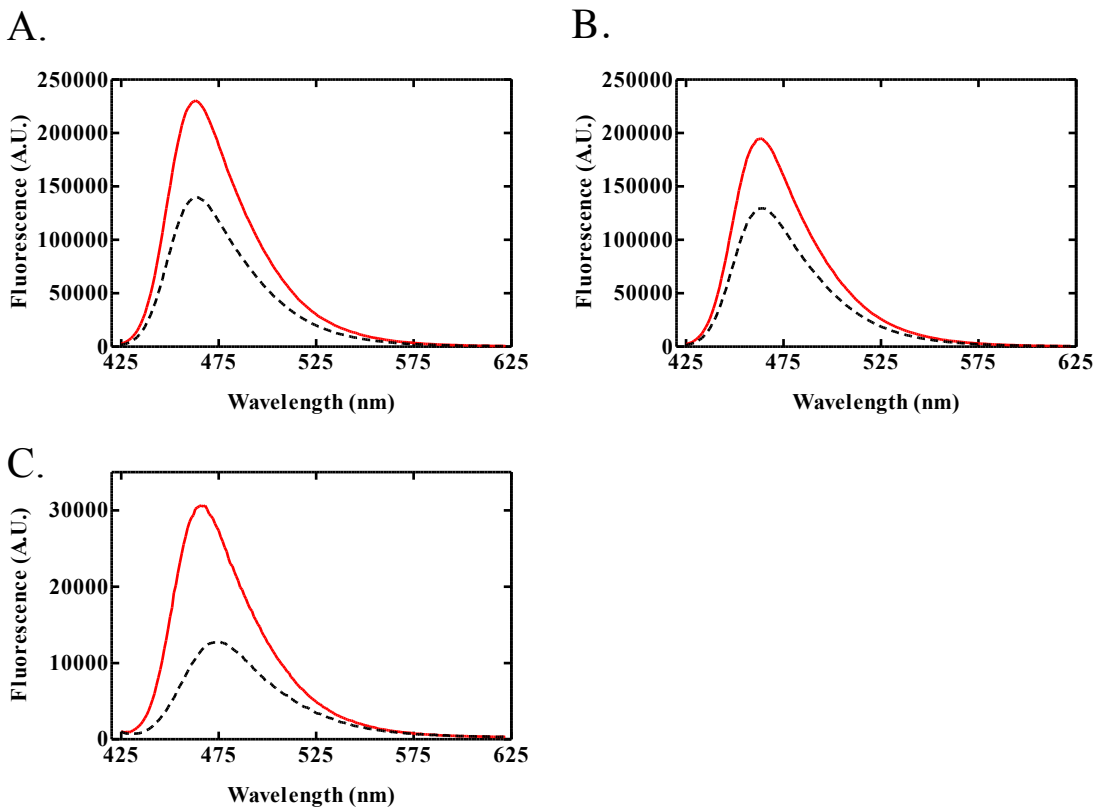

Figure 4.1. PhoS A197C-MDCC produced by various methods binds P_i and produces a fluorescence signal change. Equilibrium fluorescence measurements of PhoS A197C-MDCC and Phosphate Sensor in the absence (black dashed line) or presence (red solid line) of 20-fold molar excess P_i. The labeled protein produced using the pET28b construct (A), or by the pET22b construct (B) was assayed at a protein concentration of 5 μM; whereas the Phosphate Sensor (C) was assayed at 500 nM.

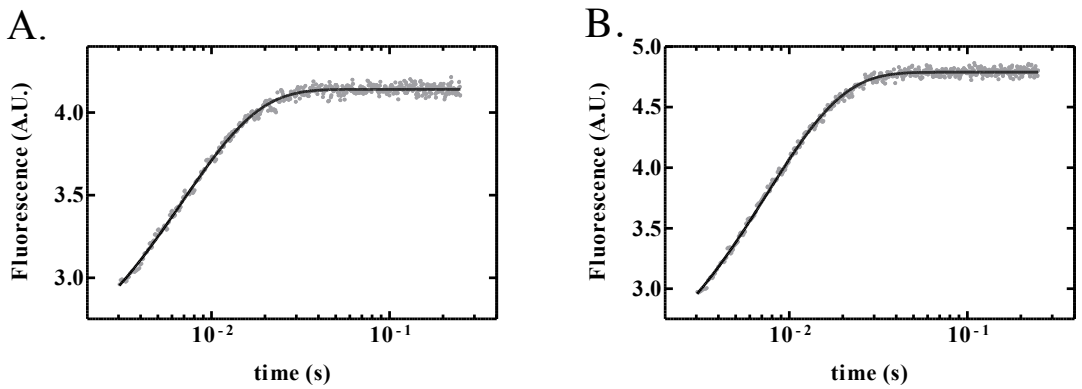

Figure 4.2. His-tagged PhoS A197C-MDCC and Phosphate Sensor produce a rapid, and large fluorescence signal change when mixed with P_i. Pre-steady state kinetics of 1.25 μM PhoS A197C-MDCC (A) or Phosphate Sensor (B) binding to 4 μM P_i. Raw data from a representative stopped-flow time course (grey dots) was fit with a one-exponential function (black line). A.U., arbitrary units.

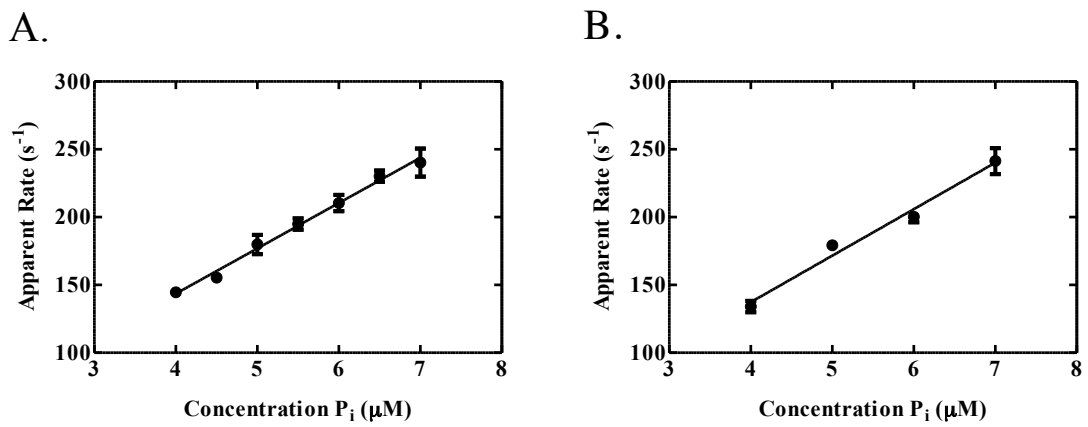

Figure 4.3. His-tagged PhoS A197C-MDCC binds phosphate as rapidly as the commercially available Phosphate Sensor. Apparent rate plots obtained from a Pi titration using (A) 1.25 μM PhoS A197C-MDCC from my preparation, or (B) 1.25 μM ThermoFisher Phosphate Sensor (n = 6 shots per data point, mean ± s.d). Slopes of the lines of best fit (k_1) were (A) 33 ± 2 $\mu M^{-1} s^{-1}$ (n = 7 data points, best fit ± s.d), and (B) 34 ± 7 $\mu M^{-1} s^{-1}$ (n = 4 data points, best fit ± s.d)

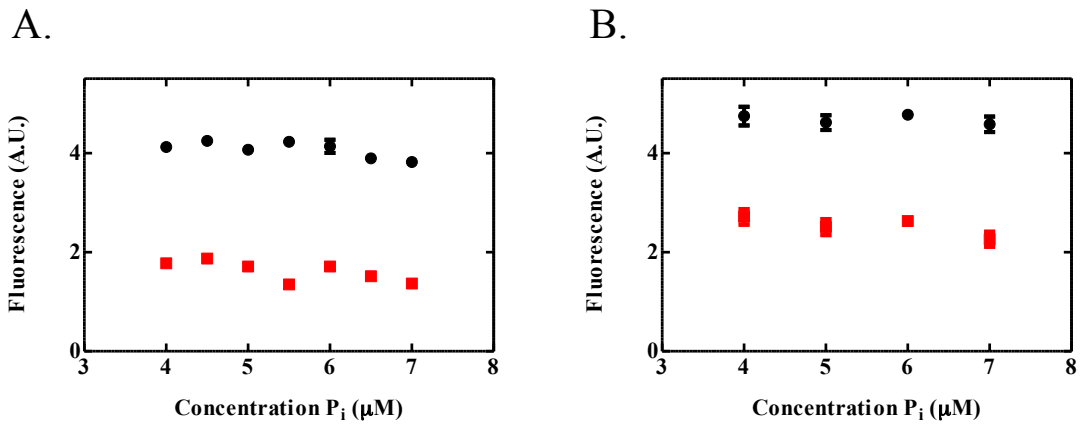

Figure 4.4. His-tagged PhoS A197C-MDCC and Phosphate Sensor provide large signal changes upon binding of P_i. Amplitude change (red squares) and final amplitude (black circles) values obtained from a Pi titration using (A) 1.25 μM PhoS A197C-MDCC from my preparation, or (B) 1.25 μM Phosphate Sensor (n = 6 shots per data point, mean ± s.d).

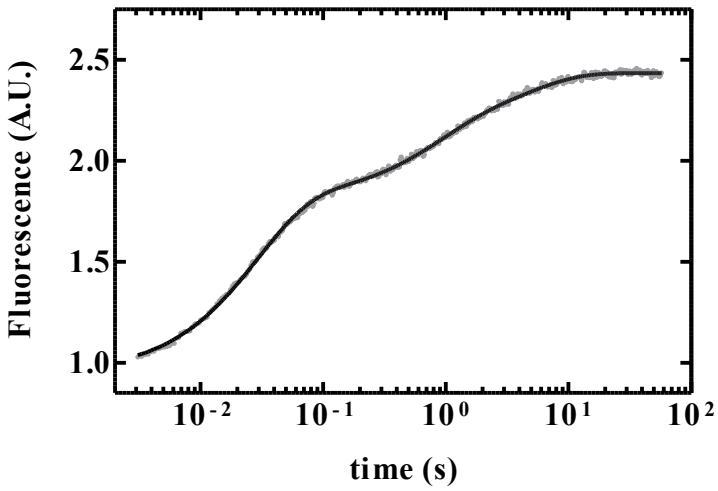

Figure 4.5. Pre-steady state kinetics of P_i release from 70S-stimulated LepA/EF4 following GTP hydrolysis. A solution of LepA/EF4 (8 μM) and GTP (120 μM) was mixed with a solution of 70S ribosomes (2 μM) and PhoS A197C-MDCC (2.5 μM). Both solutions also contained 0.1 U/mL PNP, and 200 μM 7-methylguanosine as a P_i mop. Raw data from a representative stopped-flow time course (grey dots) was fit with a three-exponential function (black line). A.U., arbitrary units.

Table 4.1. Fit parameters obtained from rapid kinetics study of P_i release from 70S-stimulated LepA/EF4 following GTP hydrolysis. A representative trace is shown with its fit in Figure 4.5. A description of the fit parameters can be found in the methods section (Equation 4.5). Values reflect the mean of best-fit parameters ± s.d. (n = 4).

Fit Parameter	Fit Value
A_1 (A.U., ± s.d.)	-0.6 ± 0.3
A_2 (A.U., ± s.d)	-0.5 ± 0.2
A_3 (A.U., ± s.d)	-0.31 ± 0.07
k_1 (s^{-1}, ± s.d.)	27 ± 9
k_2 (s^{-1}, ± s.d)	1.4 ± 0.3
k_3 (s^{-1}, ± s.d)	0.22 ± 0.04

References

Bauman, A. T., Chateauneuf, G. M., Boyd, B. R., Brown, R. E. and Murthy, P. P. (1999). "Conformational inversion processes in phytic acid: NMR spectroscopic and molecular modeling studies." Tetrahedron Letters **40**(24): 4489-4492.

Best, M. D., Zhang, H. and Prestwich, G. D. (2010). "Inositol polyphosphates, diphosphoinositol polyphosphates and phosphatidylinositol polyphosphate lipids: structure, synthesis, and development of probes for studying biological activity." Natural Product Reports **27**(10): 1403-1430.

Bretz, J. R., Mock, N. M., Charity, J. C., Zeyad, S., Baker, C. J. and Hutcheson, S. W. (2003). "A translocated protein tyrosine phosphatase of *Pseudomonas syringae pv. tomato DC3000* modulates plant defence response to infection." Molecular Microbiology **49**(2): 389-400.

Brune, M., Hunter, J. L., Corrie, J. E. and Webb, M. R. (1994). "Direct, real-time measurement of rapid inorganic phosphate release using a novel fluorescent probe and its application to actomyosin subfragment 1 ATPase." Biochemistry **33**(27): 8262-8271.

Brune, M., Hunter, J. L., Howell, S. A., Martin, S. R., Hazlett, T. L., Corrie, J. E. and Webb, M. R. (1998). "Mechanism of inorganic phosphate interaction with phosphate binding protein from *Escherichia coli*." Biochemistry **37**(29): 10370-10380.

Caffrey, J. J., Darden, T., Wenk, M. R. and Shears, S. B. (2001). "Expanding coincident signaling by PTEN through its inositol 1, 3, 4, 5, 6-pentakisphosphate 3-phosphatase activity." FEBS Letters **499**(1): 6-10.

Campbell, S., Fisher, R. J., Towler, E. M., Fox, S., Issaq, H. J., Wolfe, T., Phillips, L. R. and Rein, A. (2001). "Modulation of HIV-like particle assembly in vitro by inositol phosphates." Proceedings of the National Academy of Sciences **98**(19): 10875-10879.

Chatterjee, S., Sankaranarayanan, R. and Sonti, R. V. (2003). "PhyA, a secreted protein of *Xanthomonas oryzae pv. oryzae*, is required for optimum virulence and growth on phytic acid as a sole phosphate source." Molecular Plant-Microbe Interactions **16**(11): 973-982.

Chen, C. C., Cheng, K. J., Ko, T. P. and Guo, R. T. (2015). "Current progresses in phytase research: three‐dimensional structure and protein engineering." ChemBioEng Reviews **2**(2): 76-86.

Chu, H.-M., Guo, R.-T., Lin, T.-W., Chou, C.-C., Shr, H.-L., Lai, H.-L., Tang, T.-Y., Cheng, K.-J., Selinger, B. L. and Wang, A. H.-J. (2004). "Structures of *Selenomonas ruminantium* phytase in complex with persulfated phytate: DSP

phytase fold and mechanism for sequential substrate hydrolysis." Structure **12**(11): 2015-2024.

Coatham, M. L., Brandon, H. E., Fischer, J. J., Schümmer, T. and Wieden, H.-J. (2016). "The conserved GTPase HflX is a ribosome splitting factor that binds to the E-site of the bacterial ribosome." Nucleic Acids Research **44**(4): 1952-1961.

Craig, N., Green, R., Greider, C., Cohen-Fix, O., Storz, G. and Wolberger, C. (2014). Molecular biology: principles of genome function, OUP Oxford.

D'silva, C., Bae, H., Yanke, L., Cheng, K.-J. and Selinger, L. (2000). "Localization of phytase in *Selenomonas ruminantium* and *Mitsuokella multiacidus* by transmission electron microscopy." Canadian Journal of Microbiology **46**(4): 391-395.

De Laurentiis, E. I. and Wieden, H.-J. (2015). "Identification of two structural elements important for ribosome-dependent GTPase activity of elongation factor 4 (EF4/LepA)." Scientific Reports **5**.

Di Paolo, G. and De Camilli, P. (2006). "Phosphoinositides in cell regulation and membrane dynamics." Nature **443**(7112): 651-657.

Espinosa, A., Guo, M., Tam, V. C., Fu, Z. Q. and Alfano, J. R. (2003). "The *Pseudomonas syringae* type III‐secreted protein HopPtoD2 possesses protein tyrosine phosphatase activity and suppresses programmed cell death in plants." Molecular Microbiology **49**(2): 377-387.

Feng, J., Chen, Y., Pu, J., Yang, X., Zhang, C., Zhu, S., Zhao, Y., Yuan, Y., Yuan, H. and Liao, F. (2011). "An improved malachite green assay of phosphate: mechanism and application." Analytical Biochemistry **409**(1): 144-149.

Gasteiger, E., Hoogland, C., Gattiker, A., Duvaud, S. E., Wilkins, M. R., Appel, R. D. and Bairoch, A. (2005). Protein identification and analysis tools on the ExPASy server, Springer.

Geeves, M. A. and Holmes, K. C. (2005). "The molecular mechanism of muscle contraction." Advances in Protein Chemistry **71**: 161-193.

Goody, R. S. (2013). "How bacteria choose phosphate." Angewandte Chemie International Edition **52**: 2406-2407.

Gruninger, R. J. (2009). Structure and mechanism of protein tyrosine phosphatase-like phytases. Doctoral Thesis, University of Lethbridge, Department of Chemistry and Biochemistry, Lethbridge, AB.

Gruninger, R. J., Dobing, S., Smith, A. D., Bruder, L. M., Selinger, L. B., Wieden, H.-J. and Mosimann, S. C. (2012). "Substrate binding in protein-tyrosine phosphatase-

like inositol polyphosphatases." Journal of Biological Chemistry **287**(13): 9722-9730.

Gruninger, R. J., Goodman, R. P. and Selinger, L. B. (2003). Further evidence for a new class of phytases: Biochemical characterization of a second PTP phytase from *Mitsuokella multiacidus* 032. Annual Meeting of the Canadian Society of Microbiologists. Laval, PQ.

Gruninger, R. J., Selinger, L. B. and Mosimann, S. C. (2008). "Effect of ionic strength and oxidation on the P‐loop conformation of the protein tyrosine phosphatase‐like phytase, PhyAsr." FEBS Journal **275**(15): 3783-3792.

Gruninger, R. J., Selinger, L. B. and Mosimann, S. C. (2009). "Structural analysis of a multifunctional, tandemly repeated inositol polyphosphatase." Journal of Molecular Biology **392**(1): 75-86.

Gruninger, R. J., Thibault, J., Capeness, M. J., Till, R., Mosimann, S. C., Sockett, R. E., Selinger, B. L. and Lovering, A. L. (2014). "Structural and biochemical analysis of a unique phosphatase from *Bdellovibrio bacteriovorus* reveals its structural and functional relationship with the protein tyrosine phosphatase class of phytase." PloS One **9**(4): e94403.

Guan, K. and Dixon, J. E. (1991). "Evidence for protein-tyrosine-phosphatase catalysis proceeding via a cysteine-phosphate intermediate." Journal of Biological Chemistry **266**(26): 17026-17030.

Ha, N.-C., Oh, B.-C., Shin, S., Kim, H.-J., Oh, T.-K., Kim, Y.-O., Choi, K. Y. and Oh, B.-H. (2000). "Crystal structures of a novel, thermostable phytase in partially and fully calcium-loaded states." Nature Structural & Molecular Biology **7**(2): 147-153.

Hanakahi, L. A., Bartlet-Jones, M., Chappell, C., Pappin, D. and West, S. C. (2000). "Binding of inositol phosphate to DNA-PK and stimulation of double-strand break repair." Cell **102**(6): 721-729.

Hegeman, C. E. and Grabau, E. A. (2001). "A novel phytase with sequence similarity to purple acid phosphatases is expressed in cotyledons of germinating soybean seedlings." Plant Physiology **126**(4): 1598-1608.

Hengge, A. C., Sowa, G. A., Wu, L. and Zhang, Z.-Y. (1995). "Nature of the transition state of the protein-tyrosine phosphatase-catalyzed reaction." Biochemistry **34**(43): 13982-13987.

Hess, H. H. and Derr, J. E. (1975). "Assay of inorganic and organic phosphorus in the 0.1–5 nanomole range." Analytical biochemistry **63**(2): 607-613.

Hirshberg, M., Henrick, K., Lloyd Haire, L., Vasisht, N., Brune, M., Corrie, J. E. and Webb, M. R. (1998). "Crystal structure of phosphate binding protein labeled with

a coumarin fluorophore, a probe for inorganic phosphate." Biochemistry **37**(29): 10381-10385.

Horrocks, D. (1974). Applications of liquid scintillation counting. New York, Academic Press, Inc.

Hsieh, Y.-J. and Wanner, B. L. (2010). "Global regulation by the seven-component Pi signaling system." Current Opinion in Microbiology **13**(2): 198-203.

Huang, H., Shi, P., Wang, Y., Luo, H., Shao, N., Wang, G., Yang, P. and Yao, B. (2009). "Diversity of beta-propeller phytase genes in the intestinal contents of grass carp provides insight into the release of major phosphorus from phytate in nature." Applied and Environmental Microbiology **75**(6): 1508-1516.

Isbrandt, L. R. and Oertel, R. P. (1980). "Conformational states of myo-inositol hexakis (phosphate) in aqueous solution. A carbon-13 NMR, phosphorus-31 NMR, and Raman spectroscopic investigation." Journal of the American Chemical Society **102**(9): 3144-3148.

Johnson, M., Zaretskaya, I., Raytselis, Y., Merezhuk, Y., Mcginnis, S. and Madden, T. L. (2008). "NCBI BLAST: a better web interface." Nucleic Acids Research **36**(suppl 2): W5-W9.

Kerovuo, J., Lappalainen, I. and Reinikainen, T. (2000). "The metal dependence of *Bacillus subtilis* phytase." Biochemical and Biophysical Research Communications **268**(2): 365-369.

Klabunde, T., Sträter, N., Fröhlich, R., Witzel, H. and Krebs, B. (1996). "Mechanism of Fe (III)–Zn (II) purple acid phosphatase based on crystal structures." Journal of Molecular Biology **259**(4): 737-748.

Kostakioti, M., Newman, C. L., Thanassi, D. G. and Stathopoulos, C. (2005). "Mechanisms of protein export across the bacterial outer membrane." Journal of Bacteriology **187**(13): 4306-4314.

Kostrewa, D., Wyss, M., D'arcy, A. and Van Loon, A. P. (1999). "Crystal structure of *Aspergillus niger* pH 2.5 acid phosphatase at 2. 4 A resolution." Journal of Molecular Biology **288**(5): 965-974.

Ledvina, P. S., Yao, N., Choudhary, A. and Quiocho, F. A. (1996). "Negative electrostatic surface potential of protein sites specific for anionic ligands." Proceedings of the National Academy of Sciences **93**(13): 6786-6791.

Lim, B. L., Yeung, P., Cheng, C. and Hill, J. E. (2007). "Distribution and diversity of phytate-mineralizing bacteria." The ISME Journal **1**(4): 321-330.

Lim, D., Golovan, S., Forsberg, C. W. and Jia, Z. (2000). "Crystal structures of *Escherichia coli* phytase and its complex with phytate." Nature Structural & Molecular Biology **7**(2): 108-113.

Lionne, C., Brune, M., Webb, M. R., Travers, F. and Barman, T. (1995). "Time resolved measurements show that phosphate release is the rate limiting step on myofibrillar ATPases." FEBS Letters **364**(1): 59-62.

Liu, Q., Huang, Q., Lei, X. G. and Hao, Q. (2004). "Crystallographic snapshots of *Aspergillus fumigatus* phytase, revealing its enzymatic dynamics." Structure **12**(9): 1575-1583.

Luecke, H. and Quiocho, F. A. (1990). "High specificity of a phosphate transport protein determined by hydrogen bonds." Nature **347**(6291): 402-406.

Lupardus, P. J., Shen, A., Bogyo, M. and Garcia, K. C. (2008). "Small molecule-induced allosteric activation of the Vibrio cholerae RTX cysteine protease domain." Science **322**(5899): 265-268.

Macbeth, M. R., Schubert, H. L., Vandemark, A. P., Lingam, A. T., Hill, C. P. and Bass, B. L. (2005). "Inositol hexakisphosphate is bound in the ADAR2 core and required for RNA editing." Science **309**(5740): 1534-1539.

Macho, A. P., Schwessinger, B., Ntoukakis, V., Brutus, A., Segonzac, C., Roy, S., Kadota, Y., Oh, M.-H., Sklenar, J. and Derbyshire, P. (2014). "A bacterial tyrosine phosphatase inhibits plant pattern recognition receptor activation." Science **343**(6178): 1509-1512.

Maffucci, T., Piccolo, E., Cumashi, A., Iezzi, M., Riley, A. M., Saiardi, A., Godage, H. Y., Rossi, C., Broggini, M. and Iacobelli, S. (2005). "Inhibition of the phosphatidylinositol 3-kinase/Akt pathway by inositol pentakisphosphate results in antiangiogenic and antitumor effects." Cancer Research **65**(18): 8339-8349.

Magota, K., Otsuji, N., Miki, T., Horiuchi, T., Tsunasawa, S., Kondo, J., Sakiyama, F., Amemura, M., Morita, T. and Shinagawa, H. (1984). "Nucleotide sequence of the phoS gene, the structural gene for the phosphate-binding protein of *Escherichia coli*." Journal of Bacteriology **157**(3): 909-917.

Majerus, P. W., Zou, J., Marjanovic, J., Kisseleva, M. V. and Wilson, M. P. (2008). "The role of inositol signaling in the control of apoptosis." Advances in Enzyme Regulation **48**(1): 10-17.

Milon, P., Konevega, A. L., Peske, F., Fabbretti, A., Gualerzi, C. O. and Rodnina, M. V. (2007). "Transient kinetics, fluorescence, and FRET in studies of initiation of translation in bacteria." Methods in Enzymology **430**: 1-30.

Morita, T., Amemura, M., Makino, K., Shinagawa, H., Magota, K., Otsuji, N. and Nakata, A. (1983). "Hyperproduction of phosphate‐binding protein, phoS, and

pre‐phoS proteins in *Escherichia coli* carrying a cloned phoS gene." European Journal of Biochemistry **130**(3): 427-435.

Mullaney, E. J., Daly, C. B. and Ullah, A. (1999). "Advances in phytase research." Advances in Applied Microbiology **47**: 157-199.

Mullaney, E. J. and Ullah, A. H. (2003). "The term phytase comprises several different classes of enzymes." Biochemical and Biophysical Research Communications **312**(1): 179-184.

Murphy, A. M., Otto, B., Brearley, C. A., Carr, J. P. and Hanke, D. E. (2008). "A role for inositol hexakisphosphate in the maintenance of basal resistance to plant pathogens." The Plant Journal **56**(4): 638-652.

Murthy, P. P. (2006). Structure and nomenclature of inositol phosphates, phosphoinositides, and glycosylphosphatidylinositols. Biology of Inositols and Phosphoinositides, Springer**:** 1-19.

Oh, B.-C., Chang, B. S., Park, K.-H., Ha, N.-C., Kim, H.-K., Oh, B.-H. and Oh, T.-K. (2001). "Calcium-dependent catalytic activity of a novel phytase from *Bacillus amyloliquefaciens DS11*." Biochemistry **40**(32): 9669-9676.

Okoh, M. P., Hunter, J. L., Corrie, J. E. and Webb, M. R. (2006). "A biosensor for inorganic phosphate using a rhodamine-labeled phosphate binding protein." Biochemistry **45**: 14764-14771.

Orchiston, E. A., Bennett, D., Leslie, N. R., Clarke, R. G., Winward, L., Downes, C. P. and Safrany, S. T. (2004). "PTEN M-CBR3, a versatile and selective regulator of inositol 1, 3, 4, 5, 6-pentakisphosphate (Ins (1, 3, 4, 5, 6) P5) evidence for Ins (1, 3, 4, 5, 6) P5 as a proliferative signal." Journal of Biological Chemistry **279**(2): 1116-1122.

Ostanin, K., Harms, E. H., Stevis, P. E., Kuciel, R., Zhou, M.-M. and Van Etten, R. (1992). "Overexpression, site-directed mutagenesis, and mechanism of *Escherichia coli* acid phosphatase." Journal of Biological Chemistry **267**(32): 22830-22836.

Ostanin, K. and Van Etten, R. (1993). "Asp304 of *Escherichia coli* acid phosphatase is involved in leaving group protonation." Journal of Biological Chemistry **268**(28): 20778-20784.

Pannifer, A. D., Flint, A. J., Tonks, N. K. and Barford, D. (1998). "Visualization of the cysteinyl-phosphate intermediate of a protein-tyrosine phosphatase by X-ray crystallography." Journal of Biological Chemistry **273**(17): 10454-10462.

Petersen, T. N., Brunak, S., Von Heijne, G. and Nielsen, H. (2011). "SignalP 4.0: discriminating signal peptides from transmembrane regions." Nature Methods **8**(10): 785-786.

Piccolo, E., Vignati, S., Maffucci, T., Innominato, P. F., Riley, A. M., Potter, B. V., Pandolfi, P. P., Broggini, M., Iacobelli, S. and Innocenti, P. (2004). "Inositol pentakisphosphate promotes apoptosis through the PI 3-K/Akt pathway." Oncogene **23**(9): 1754-1765.

Posor, Y., Eichhorn-Gruenig, M., Puchkov, D., Schöneberg, J., Ullrich, A., Lampe, A., Müller, R., Zarbakhsh, S., Gulluni, F. and Hirsch, E. (2013). "Spatiotemporal control of endocytosis by phosphatidylinositol-3, 4-bisphosphate." Nature **499**(7457): 233-237.

Puhl, A. A., Greiner, R. and Selinger, L. B. (2008a). "Kinetics, substrate specificity, and stereospecificity of two new protein tyrosine phosphatase-like inositol polyphosphatases from *Selenomonas lacticifex*." Biochemistry and Cell Biology **86**(4): 322-330.

Puhl, A. A., Greiner, R. and Selinger, L. B. (2008b). "A protein tyrosine phosphatase-like inositol polyphosphatase from *Selenomonas ruminantium subsp. lactilytica* has specificity for the 5-phosphate of myo-inositol hexakisphosphate." The International Journal of Biochemistry & Cell Biology **40**(10): 2053-2064.

Puhl, A. A., Greiner, R. and Selinger, L. B. (2009). "Stereospecificity of myo-inositol hexakisphosphate hydrolysis by a protein tyrosine phosphatase-like inositol polyphosphatase from *Megasphaera elsdenii*." Applied Microbiology and Biotechnology **82**(1): 95-103.

Puhl, A. A., Gruninger, R. J., Greiner, R., Janzen, T. W., Mosimann, S. C. and Selinger, L. B. (2007). "Kinetic and structural analysis of a bacterial protein tyrosine phosphatase‐like myo‐inositol polyphosphatase." Protein Science **16**(7): 1368-1378.

Qin, Y., Polacek, N., Vesper, O., Staub, E., Einfeldt, E., Wilson, D. N. and Nierhaus, K. H. (2006). "The highly conserved LepA is a ribosomal elongation factor that back-translocates the ribosome." Cell **127**(4): 721-733.

Quignard, J., Rakotoarisoa, L., Mironneau, J. and Mironneau, C. (2003). "Stimulation of L‐type Ca2+ channels by inositol pentakis‐and hexakisphosphates in rat vascular smooth muscle cells." The Journal of Physiology **549**(3): 729-737.

Raboy, V. and Dickinson, D. B. (1987). "The timing and rate of phytic acid accumulation in developing soybean seeds." Plant Physiology **85**(3): 841-844.

Ragon, M., Hoh, F., Aumelas, A., Chiche, L., Moulin, G. and Boze, H. (2009). "Structure of *Debaryomyces castellii* CBS 2923 phytase." Acta Crystallographica Section F: Structural Biology and Crystallization Communications **65**(4): 321-326.

Reddy, N., Sathe, S. and Salunkhe, D. (1982). "Phytates in legumes and cereals." Advances in Food Research **28**(1): 1-92.

Rossburger, N. G., Smith, A. D., Gruninger, R. J. and Selinger, L. B. (2012). Not all Protein Tyrosine Phosphatase like Phytases have a narrow substrate specificity. Annual Meeting of the Canadian Society of Microbiologists, Vancouver BC.

Savelsbergh, A., Mohr, D., Kothe, U., Wintermeyer, W. and Rodnina, M. V. (2005). "Control of phosphate release from elongation factor G by ribosomal protein L7/12." The EMBO Journal **24**(24): 4316-4323.

Shi, L., Potts, M. and Kennelly, P. J. (1998). "The serine, threonine, and/or tyrosine‐specific protein kinases and protein phosphatases of prokaryotic organisms: A family portrait." FEMS Microbiology Reviews **22**(4): 229-253.

Shields, M. J., Fischer, J. J. and Wieden, H.-J. (2009). "Toward understanding the function of the universally conserved GTPase HflX from Escherichia coli: a kinetic approach." Biochemistry **48**(45): 10793-10802.

Solscheid, C., Kunzelmann, S., Davis, C. T., Hunter, J. L., Nofer, A. and Webb, M. R. (2015). "Development of a reagentless biosensor for inorganic phosphate, applicable over a wide concentration range." Biochemistry **54**(32): 5054-5062.

Steger, D. J., Haswell, E. S., Miller, A. L., Wente, S. R. and O'shea, E. K. (2003). "Regulation of chromatin remodeling by inositol polyphosphates." Science **299**(5603): 114-116.

Streb, H., Irvine, R., Berridge, M. and Schulz, I. (1983). "Release of Ca2+ from a nonmitochondrial intracellular store in pancreatic acinar cells by inositol-1, 4, 5-trisphosphate." Nature **306**(5938): 67-69.

Takagi, Y., Shuman, H. and Goldman, Y. (2004). "Coupling between phosphate release and force generation in muscle actomyosin." Philosophical Transactions of the Royal Society B: Biological Sciences **359**(1452): 1913-1920.

Tan, X., Calderon-Villalobos, L. I. A., Sharon, M., Zheng, C., Robinson, C. V., Estelle, M. and Zheng, N. (2007). "Mechanism of auxin perception by the TIR1 ubiquitin ligase." Nature **446**(7136): 640-645.

Thibault, J. (2010). The characterization of two novel PTP-like enzymes from *Bdellovibrio bacteriovorus* and *Pseudomonas syringae* pv. tomato DC3000. Master's Thesis, University of Lethbridge, Department of Biological Sciences, Lethbridge, AB.

Thompson, J. D., Higgins, D. G. and Gibson, T. J. (1994). "CLUSTAL W: improving the sensitivity of progressive multiple sequence alignment through sequence weighting, position-specific gap penalties and weight matrix choice." Nucleic Acids Research **22**(22): 4673-4680.

Trentham, D., Bardsley, R., Eccleston, J. and Weeds, A. (1972). "Elementary processes of the magnesium ion-dependent adenosine triphosphatase activity of heavy

meromysin. A transient kinetic approach to the study of kinases and adenosine triphosphatases and a colorimetric inorganic phosphate assay *in situ*." Biochemical Journal **126**(3): 635-644.

Ullah, A. H. and Cummins, B. J. (1988). "*Aspergillus ficuum* extracellular pH 6.0 optimum acid phosphatase: purification, N-terminal amino acid sequence, and biochemical characterization." Preparative Biochemistry **18**(1): 37-65.

Van Hartingsveldt, W., Van Zeijl, C. M., Harteveld, G. M., Gouka, R. J., Suykerbuyk, M. E., Luiten, R. G., Van Paridon, P. A., Selten, G. C., Veenstra, A. E. and Van Gorcom, R. F. (1993). "Cloning, characterization and overexpression of the phytase-encoding gene (phyA) of *Aspergillus niger*." Gene **127**(1): 87-94.

Van Herk, P. (2014). Specificity of a novel myo-inositol phosphatase towards less-phosphorylated myo-inositol phosphates. Master's Thesis, University of Lethbridge, Department of Chemistry and Biochemistry, Lethbridge, AB.

Van Herk, P., Rossburger, N., Smith, A., Mosimann, S. and Selinger, B. (2015). Is Phytase A from *Myxococcus stipitatus* involved in scavenging phosphate? 11th Annual International Symposium on Biocatalysis and Agricultural Biotechnology, Banff AB.

Wang, Q., Arnold, J. J., Uchida, A., Raney, K. D. and Cameron, C. E. (2010). "Phosphate release contributes to the rate-limiting step for unwinding by an RNA helicase." Nucleic Acids Research **38**(4): 1312-1324.

Weber, S., Stirnimann, C. U., Wieser, M., Frey, D., Meier, R., Engelhardt, S., Li, X., Capitani, G., Kammerer, R. A. and Hilbi, H. (2014). "A type IV translocated Legionella cysteine phytase counteracts intracellular growth restriction by phytate." Journal of Biological Chemistry **289**(49): 34175-34188.

Wilden, B., Savelsbergh, A., Rodnina, M. V. and Wintermeyer, W. (2006). "Role and timing of GTP binding and hydrolysis during EF-G-dependent tRNA translocation on the ribosome." Proceedings of the National Academy of Sciences **103**(37): 13670-13675.

Willsky, G. R. and Malamy, M. H. (1980). "Characterization of two genetically separable inorganic phosphate transport systems in *Escherichia coli*." Journal of Bacteriology **144**(1): 356-365.

Wu, L. and Zhang, Z.-Y. (1996). "Probing the function of Asp128 in the low molecular weight protein-tyrosine phosphatase-catalyzed reaction. A pre-steady-state and steady-state kinetic investigation." Biochemistry **35**(17): 5426-5434.

Wymann, M. P. and Schneiter, R. (2008). "Lipid signalling in disease." Nature Reviews Molecular Cell Biology **9**(2): 162-176.

Yanke, L., Bae, H., Selinger, L. and Cheng, K. (1998). "Phytase activity of anaerobic ruminal bacteria." Microbiology **144**(6): 1565-1573.

Yanke, L., Selinger, L. and Cheng, K. J. (1999). "Phytase activity of *Selenomonas ruminantium*: a preliminary characterization." Letters in Applied Microbiology **29**(1): 20-25.

York, J. D., Odom, A. R., Murphy, R., Ives, E. B. and Wente, S. R. (1999). "A phospholipase C-dependent inositol polyphosphate kinase pathway required for efficient messenger RNA export." Science **285**(5424): 96-100.

Zhang, Z.-Y. (2003). "Mechanistic studies on protein tyrosine phosphatases." Progress in Nucleic Acid Research and Molecular Biology **73**: 171-220.